Substituent effects and Mechanism Studies in CO2 Transformation to Benzoxazinone Derivatives as Worthwhile N-containing Heterocycles: insight from DFT simulation

Mohammad Izadyar (izadyar@um.ac.ir)
Ferdowsi University of Mashhad https://orcid.org/0000-0002-3795-9982
Hossein Sabet-Sarvestani
Ferdowsi University of Mashhad
Hossein Eshghi
Ferdowsi University of Mashhad

Research Article

Keywords: Carbon dioxide, Benzoxazinones, Energetic span model, Electron localization function

Posted Date: February 12th, 2021

DOI: https://doi.org/10.21203/rs.3.rs-214656/v1

Substituent effects and Mechanism Studies in CO_2 Transformation to Benzoxazinone Derivatives as Worthwhile N-containing Heterocycles: insight from DFT simulation

Hossein Sabet-Sarvestani, Hossein, Eshghi, and Mohammad Izadyar *

** Correspondence to Mohammad Izadyar.(E-mail address: izadyar@um.ac.ir)*

Abstract

Investigation of CO_2 transformation into value-added organic molecules is an interesting purpose in scientific communities. Here, the substitute effect exploration in CO_2 incorporation reaction toward benzoxazinones formation, as a bioactive heterocyclic compound, is the main studied issue. A profound understanding of the substituent effect is helpful toward the investigation of the kinetic and thermodynamic aspects of the reaction. The substituted arynes, an imine compound, and atmospheric CO_2 have been reported as the starting reactants. The substituted functional groups show substantial consequences on the studied mechanisms. The obtained results show that mechanism A, in which the imine compound is added as a nucleophile to arynes, is the most probable mechanism. The Energetic Span Model (ESM) was used in the kinetic studies, which indicates the turnover-frequency determining intermediate (TDI) and turnover-frequency determining transition state (TDTS) in the reaction progress. Also, Electron localization function (ELF) analyses reveal that the electron density of a developing monosynaptic basin on the carbon atom (V(C)) at the transition state shows a good linear correlation with the calculated energy values of TDTS. Electron-withdrawing and electron-releasing characters of the substituents have the main effects on the electron density of the developing basin at the transition states which change the TDTS energies.

Keywords: Carbon dioxide; Benzoxazinones; Energetic span model; Electron localization function.

Introduction

Human activities such, as burning fossil fuels for power production, manufacturing, and transportation are the origin of greenhouse gases emission. Regarding the reports, the CO_2 amount grows up from 280 ppm (parts per million) in the mid-1800s to 397 ppm in 2014, which shows an average growth of 2 ppm/year in the last 10 years [1]. Global warming, ocean acidification, and CO_2 fertilization are harmful consequences of unusual CO_2 emissions. To attain sustainable development, an effective understanding of increasing environmental problems and global climate-changing is necessary. Thus, practical approach innovations, such as climate change inhabitation, environment conservation and fossil fuel replacement by green energies, must be considered by

scientific communities. However, in addition to reducing fossil fuel usage and change in the energy resource, CO_2 capture and utilization as a feedstock to produce value-added compounds are other developing solutions among scientists [2,3]. CO_2 utilization, as a C1 source, has great direct or indirect potential uses. The direct use of CO_2 includes CO_2-enhanced oil recovery, beverage carbonation, food processing, the cleaning agent in the textile, etc., which have been applied for several decades [4]. However, the extent of these usages is small.

CO_2 can be transformed into various value-added chemicals such as formic acid [5], carboxylated structures [6,7], inorganic carbonates, ethylene/propylene carbonates, polycarbonates [8-11], biodegradable polymers [12-14], and various heterocycles [15-19]. A range of technologies based on CO_2 conversion for various product manufacturing was proposed [20]. CO_2, as an alternative to phosgene or carbon monoxide, is applied in the synthesis of heterocycles, which are the building block of the N-containing heterocyclic compound synthesis, such as oxazolidinones [21], imidazolidinones [22], quinazolines [23-25], etc.

N-containing heterocycles, as the biocompatible compounds, are used as pharmaceutical and agrochemical agents [26-28]. The derivatives such as benzothiazoles, benzimidazoles, and benzoxazinone, are typical N-containing heterocycles that are extensively used as an antiviral, antibacterial, anticancer, antifungal, antibacterial agent, antihypertensive, and anti-inflammatory [29-32]. CO_2 incorporation by nucleophiles, as an efficient and green approach in heterocycle synthesis, has been investigated in recent years, frequently [33]. Based on the reports, CO_2 incorporation can be progressed through three routes including (1) nucleophilic addition to CO_2 followed by intramolecular cyclization to carboxylated cycle production; (2) concerted two-nucleophilic site attacks on CO_2 affording cyclic carbonyl compound; (3) cyclization due to nucleophilic attack on the reduced CO_2 [33].

Yoshida and coworker reported a CO_2 incorporation reaction in the six-membered heterocycle formation by using arynes and imines, which produces benzoxazinone compounds [34]. Arynes possess different electron-releasing and electron-withdrawing substituents, which afford distinct effects on the thermodynamic and kinetic behaviors of the benzoxazinone formation. The substituents have different effects on the hydrogen-less carbon atom of arynes as meta and para positions. Based on the Yoshida report, a zwitterion is obtained from the nucleophilic addition of imines to arynes, which is an excellent molecular scaffold for CO_2 capture. The aryne functional groups have undeniable effects on the CO_2 incorporation. Here, based on the previous experiences [35-40], a comprehensive mechanism study was performed on the benzoxazinone formation, consists of two separate routes for the reaction progress. According to the obtained theoretical results at two computational levels, meta and para positions on the arynes have different behaviors against CO_2 or imines. The Energetic Span

Model (ESM), as a kinetic-quantum chemical model, was used to investigate the kinetic aspects of the reaction. Also, powerful quantum chemistry descriptors, such as Electron Localization Function (ELF) and Fukui Functions are applied to describe the observed substituent behavior in the reaction. Fig. 1 shows the overall reaction and the studied substituted arynes in the reaction.

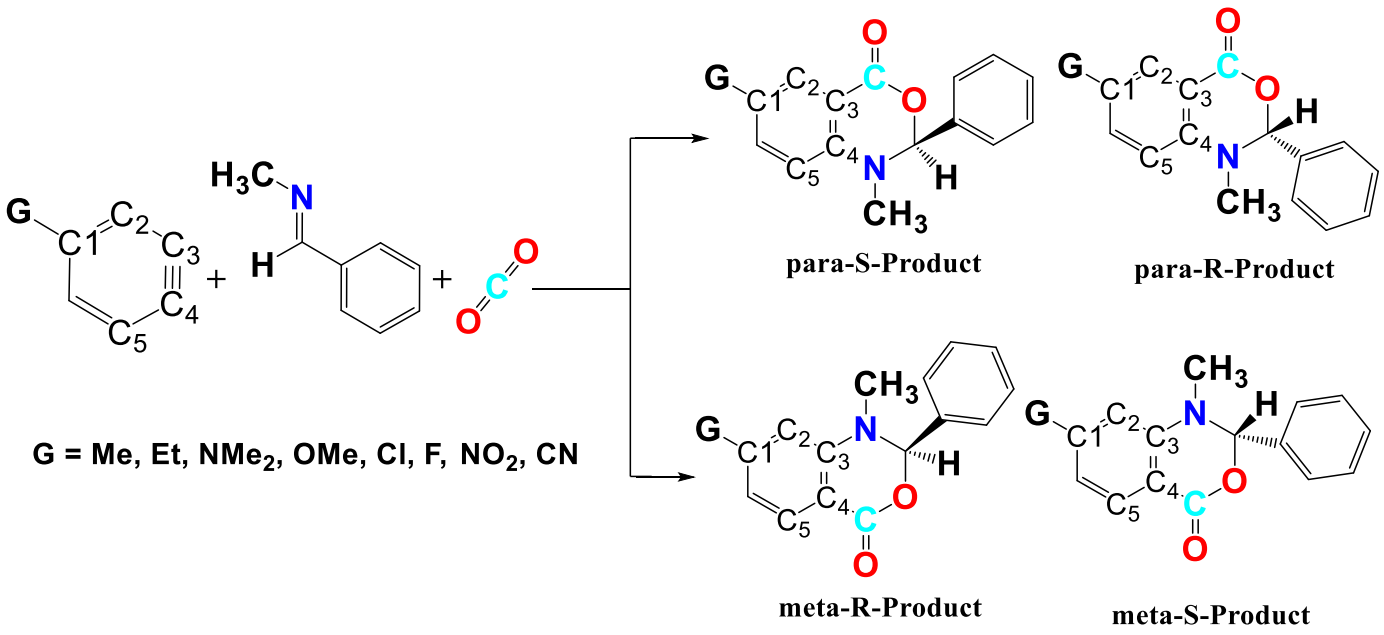

Fig. 1 The overall reaction, and the substituted arynes, within atom numbering for the involved atoms in the reaction

Computational details

Geometry optimization and vibrational frequency calculations were carried out using M06-2X functional [41] by the Gaussian 09 software [42]. The calculations were performed by two different basis sets of 6-31+G(d,p) and 6-311++G(2d,p) [43,44]. According to Schlegel's synchronous transit-guided quasi-Newton method (STQN), the structures of the transition states (TSs) were located and their accuracies were checked via the intrinsic reaction coordinate (IRC) calculations to specify the connection of the TS structure to the corresponding products and reactants [45]. The stationary points were determined by vibrational frequency calculations to check that the calculated reactants and products have positive vibrational frequencies and the TSs have only one imaginary frequency. The zero-point vibrational energy (ZPVE) correction was applied for the calculated thermodynamic and kinetic parameters based on the harmonic oscillator approximation and solvation corrections at 298.15 K and 1 atm. The solvent effects were evaluated in tetrahydrofuran (THF) as the solvent by conductor-like polarizable continuum model (CPCM) [46]. This method defines the cavity as a group of nuclear-centered spheres within a dielectric continuum. Topological analysis of the ELF was obtained by MultiWFN package [47].

Results and discussions

Two distinct mechanisms can be considered for the reaction, determined by A and B letters. Mechanism A is initiated by the nucleophilic addition of imine to meta/para position, while in mechanism B, it is assumed that the substituted arynes behave as the nucleophile species (Fig. 2). **In1A** and **In2A**, in which the electron density of the lone pair electrons are on the C3 and C4 atoms, are the outcomes of steps 1A and 1A', respectively. In steps 2A and 2A', CO_2 molecule incorporates to C3 or C4 atoms, yielding **In2** and **In2'**, respectively, which are the common intermediates in both mechanisms. Steps 3 and 3', as the final steps of both mechanisms, are intramolecular nucleophilic additions, which proceed through different paths including ***si*** face and ***re*** face states. Indeed, according to Cahn-Ingold-Prelog sequence rules [48], linked carbon atoms to nitrogen (iminic carbon) of **In2** and **In2'** are prochiral centers, in which nucleophilic species can be added to two different faces (Fig. 3). The outcomes of the ***re*** face approaching in both intermediates are two diastereomers with S configurations, and vice versa R configurations diastereomers for the ***si*** face approaching mode.

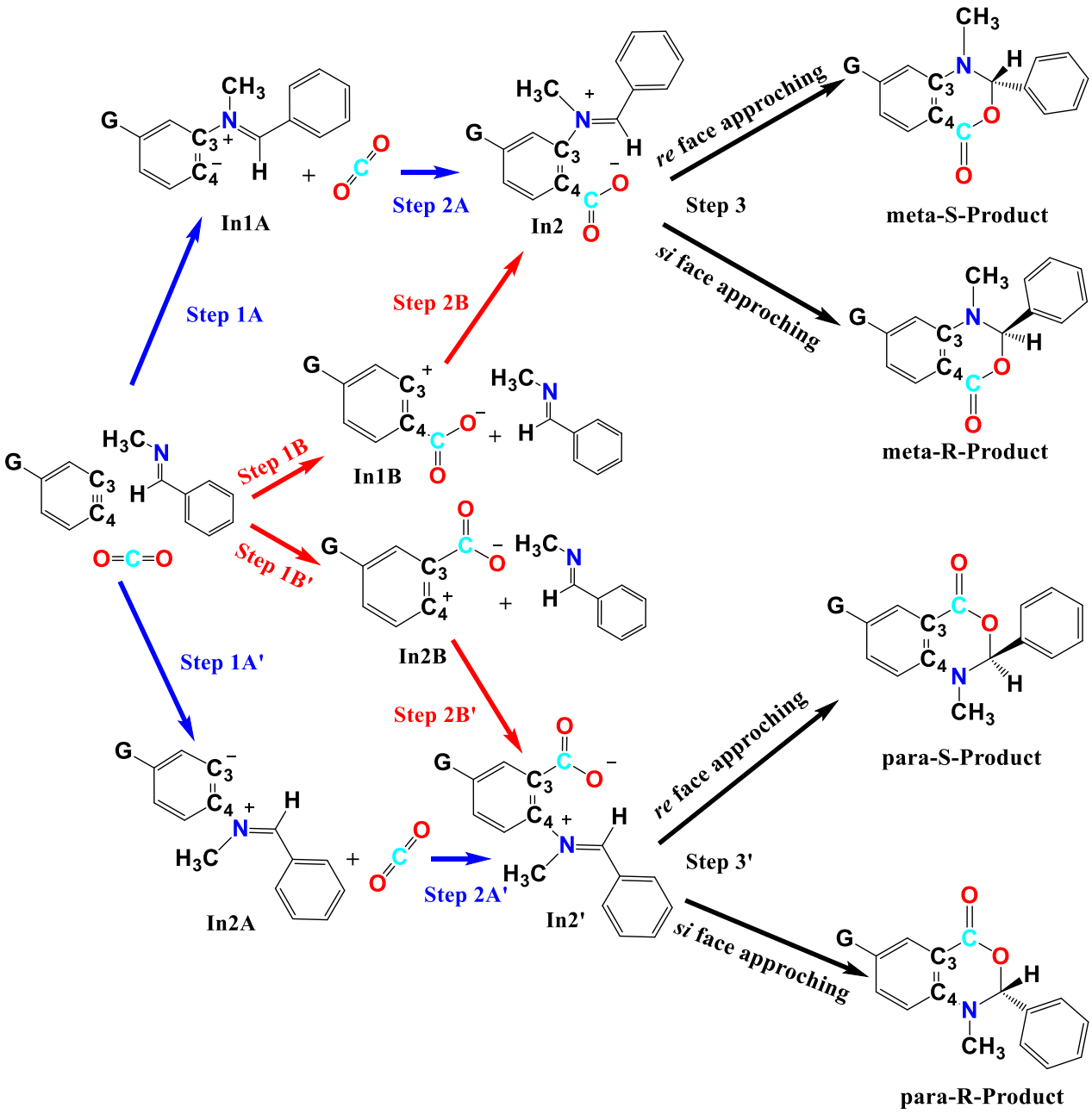

Fig. 2 Two possible mechanisms: mechanism A (blue lines) and mechanism B (red lines). Black lines illustrate the common steps of both mechanisms

However, in mechanism B, arynes act as nucleophiles, in which the nucleophilic addition to the carbon atom of CO_2 leads to **In1B** and **In2B** formation. The bond formation between the electron-deficient carbon atoms of **In1B** and **In2B** and lone pair electrons of the iminic nitrogen atom in steps 2B and 2B' produces **In2** and **In2'**. However, the obtained results in both calculated methods show that mechanism B is not a favorable mechanism for the reaction progress. Indeed, the optimized intermediates and transition states for some electron-withdrawing functional groups, such as CN, NO_2, Cl, and F are not achievable and all efforts to get their optimization structures were failed.

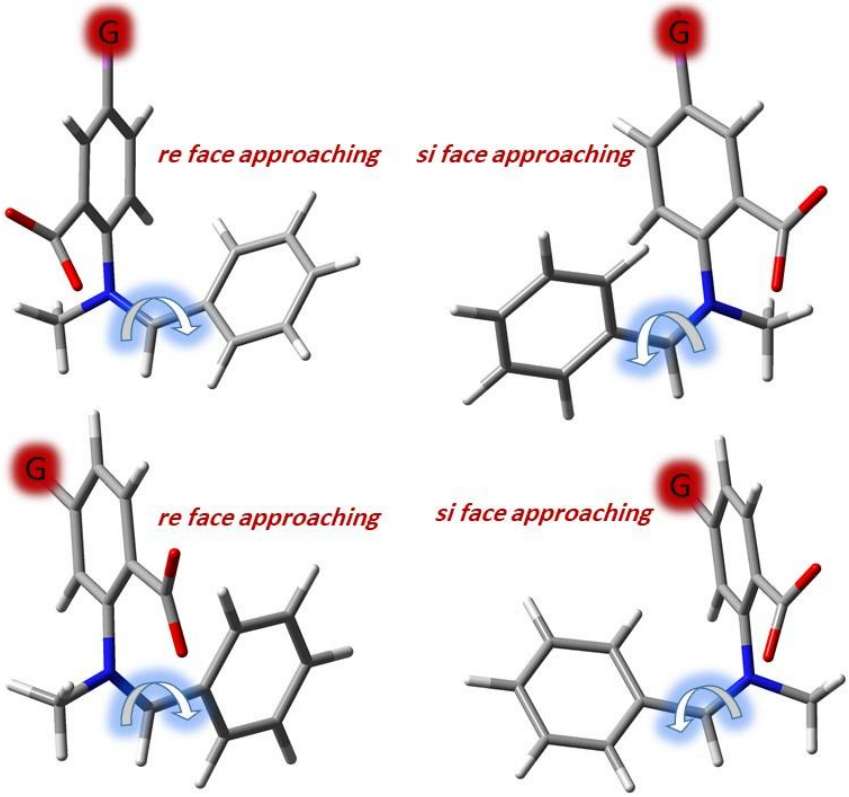

Fig. 3 Different nucleophile approaching modes in steps 3 and 3'

Mechanism B is only probable for limited functional groups, such as Et, Me, OMe and NMe_2. It can be concluded that the nucleophilic behavior of arynes against CO_2 molecule can be considered only for those having electron-releasing groups. Therefore, the local nucleophilicity of the involved arynes atoms in the reaction has a considerable difference.

Local nucleophilicity (N_k) (Eq(1)), at the atomic k position, can be defined by the related condensed Fukui functions, f_k^- (Eq(2)), in which $q_k(N)$ and $q_k(N-1)$ are natural atomic charges of the N and N-1 electronic states [49]. *N*, as the global nucleophilicity index, is calculated by Eq(3), in which $E_{HOMO\,(Nu)}$ and $E_{HOMO\,(TCE)}$ are the HOMO energies of the substituted arynes (nucleophilic species), and tetracyanoethylene (TCE), respectively. Global nucleophilicity is defined relative to TCE because it shows the lowest HOMO energy in the large series of molecules [49]. Table 1 represents the HOMO energies of the substituted arynes, natural atomic charges of N and N-1 electronic states for C3 and C4 atoms, calculated f_k^-, and *N*. Fig. 4 depicts the donor (nucleophilic) Fukui function isosurfaces and the obtained N_k for C3 and C4 atoms.

$$N_k = N.f_k^- \qquad Eq(1)$$

$$f_k^- = q_k(N-1) - q_k(N) \qquad Eq(2)$$

$$N = E_{HOMO(Nu)}(eV) - E_{HOMO(TCE)}(eV) \qquad Eq(3)$$

As shown in Fig. 4, N_k values for C3 and C4 atoms of arynes having electron-withdrawing substituents are substantially lower than the others. Therefore, the nucleophilicity character of these atoms in the substituted arynes by NO_2, CN, F, and Cl groups is lower than that of Et, Me, OMe, and NMe_2. It is a logical reason for the justification of failed attempts to the optimization of intermediates and transition states in the substituted arynes owning electron-withdrawing groups.

Table 1 HOMO energies (eV) of the substituted arynes, natural atomic charges of N and N-1 electronic states for C3 and C4 atoms, calculated f_k^-, and *N* (eV)

	G	E_{HOMO}	q_N(C3)	q_N(C4)	q_{N-1}(C3)	q_{N-1}(C4)	*N*	f_k^-(C3)	f_k^-(C4)
6-31+G(d,p)	F	-0.3221	0.0141	0.0156	0.0559	0.0815	0.0629	0.0418	0.0659
	Cl	-0.3175	0.0144	0.0260	0.0551	0.0927	0.0675	0.0407	0.0667
	NO_2	-0.3473	0.0139	0.0663	0.0585	0.1161	0.0377	0.0447	0.0498
	CN	-0.3381	0.0046	0.0613	0.0538	0.1142	0.0469	0.0493	0.0529
	Et	-0.3109	0.0163	-0.0132	0.0739	0.0525	0.0741	0.0576	0.0657
	Me	-0.3108	0.0160	-0.0129	0.0717	0.0518	0.0742	0.0557	0.0646
	OMe	-0.2915	0.0270	-0.0215	0.0720	0.0527	0.0935	0.0450	0.0742
	NMe_2	-0.2543	0.0449	-0.0596	0.0952	0.0230	0.1307	0.0503	0.0825
	TCE	-0.3850							
6-311++G(2d,p)	F	-0.3231	0.0128	0.0177	0.0520	0.0817	0.0655	0.0418	0.0659
	Cl	-0.3181	0.0139	0.0273	0.0477	0.0971	0.0705	0.0407	0.0667
	NO_2	-0.3495	0.0113	0.0694	0.0591	0.1173	0.0392	0.0447	0.0498
	CN	-0.3401	0.0033	0.0650	0.0541	0.1144	0.0485	0.0493	0.0529
	Et	-0.3121	0.0170	-0.0138	0.0719	0.0485	0.0765	0.0576	0.0657
	Me	-0.3122	0.0170	-0.0137	0.0714	0.0483	0.0764	0.0557	0.0646
	OMe	-0.2929	0.0289	-0.0219	0.0714	0.0481	0.0957	0.0450	0.0742
	NMe_2	-0.2566	0.0474	-0.0601	0.0943	0.0197	0.1320	0.0503	0.0825
	TCE	-0.3886							

Tables 2 and 1(S) represent the calculated thermodynamic and kinetic parameters for different steps of mechanisms A and B, respectively. The calculated activation Gibbs energy ($\Delta G^{\neq}$) for step 1 of both mechanisms shows that mechanism B is not a favorable mechanism. Indeed, the nucleophilic character of the substituted arynes versus CO_2 is substantially lower than that of imines. Therefore, the reaction progress through the nucleophilic addition of imines is the most probable mechanism.

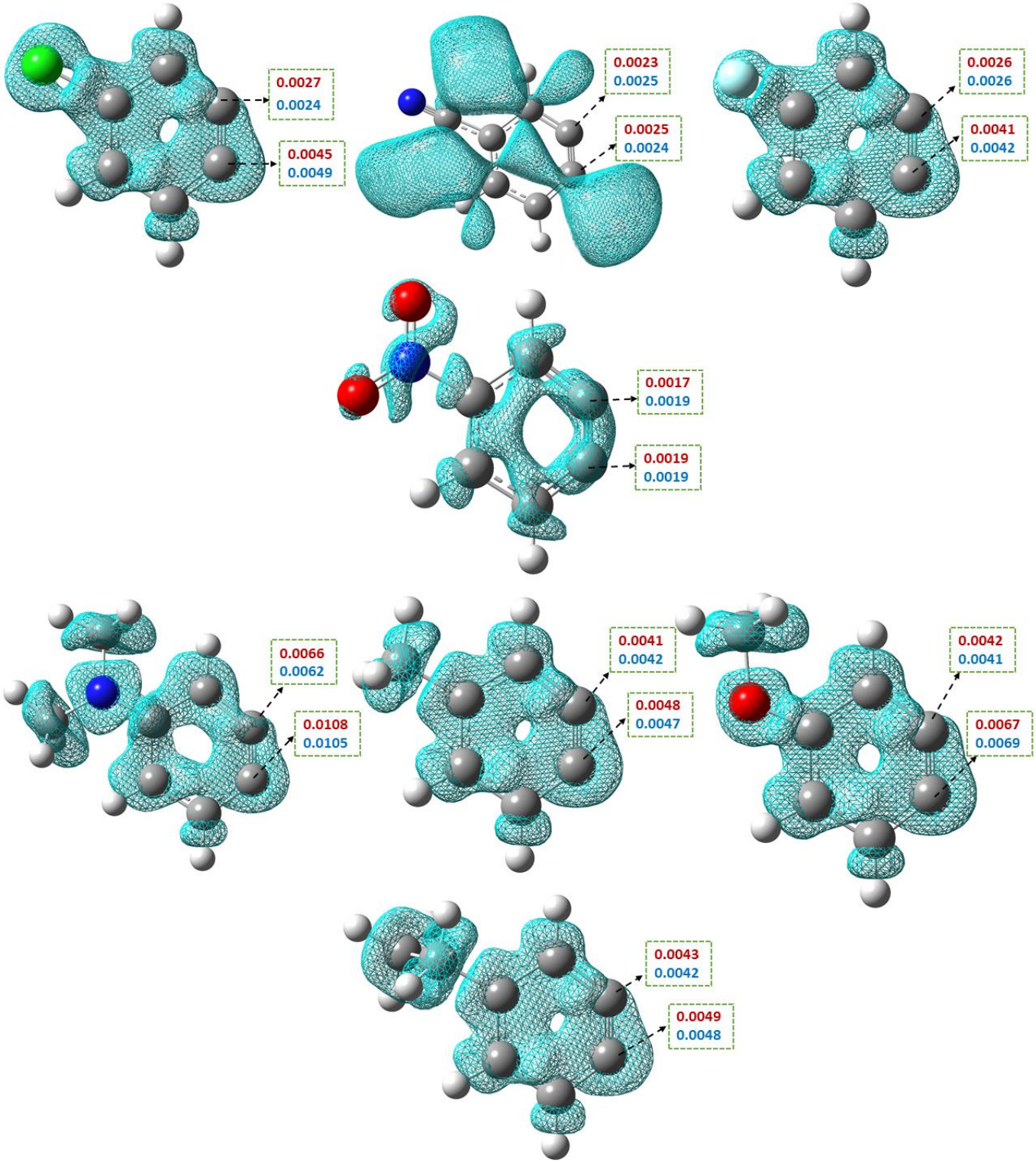

Fig. 4 Donor (nucleophilic) Fukui functions isosurfaces and nucleophilicity indexes (N_k) (e) for C4 and C5 atoms at M06-2X/6-31+G(d,p) (Blue color) and M06-2X/6-311++G(2d,p) (Red color) levels.

Table 2 Thermodynamic and kinetic parameters of the reaction steps for mechanism A

			F				Me				Et				NMe_2			
	Steps		ΔG^1	ΔH^1	ΔS^2	$\Delta G^{\neq 1}$	ΔG^1	ΔH^1	ΔS^2	$\Delta G^{\neq 1}$	ΔG^1	ΔH^1	ΔS^2	$\Delta G^{\neq 1}$	ΔG^1	ΔH^1	ΔS^2	$\Delta G^{\neq 1}$
Mechanism A	1A		-22.19	-26.18	-13.39	3.26	-18.79	-24.82	-20.22	4.65	-18.67	-24.88	-20.82	5.43	-19.47	-24.91	-18.24	3.97
	1A'		-24.69	-28.53	-12.87	3.26	-19.16	-25.21	-20.29	5.08	-19.29	-25.10	-19.47	5.19	-21.31	-26.42	-17.14	4.88
	2A		-33.93	-44.50	-35.46	-	-35.20	-47.41	-40.97	-	-35.75	-46.66	-36.60	-	-37.95	-48.95	-36.87	-
	2A'		-31.94	-42.91	-36.79	-	-34.35	-46.97	-42.31	-	-35.58	-46.38	-36.22	-	-36.79	-47.73	-36.69	-
6-31+G(d,p)	3	re	-19.46	-21.38	-6.44	1.99	-19.21	-19.84	-2.11	1.77	-18.57	-20.19	-5.45	2.10	-20.50	-22.11	-5.39	1.66
		si	-19.47	-21.38	-6.42	1.99	-19.21	-19.84	-2.11	0.88	-19.21	-20.31	-3.69	1.97	-20.50	-22.11	-5.38	1.02
	3'	re	-17.29	-19.14	-6.21	1.92	-20.04	-19.49	1.84	1.64	-17.45	-19.67	-7.42	2.42	-15.40	-17.30	-6.40	1.81
		si	-17.28	-19.14	-6.22	1.92	-19.52	-19.16	1.23	1.61	-17.84	-20.16	-7.78	1.94	-16.02	-18.10	-6.99	1.85
	1A		-20.11	-25.64	-18.55	4.15	-17.12	-19.90	-9.34	4.28	-19.02	-21.88	-9.60	3.81	-17.44	-22.98	-18.58	4.46
	1A'		-22.36	-27.94	-18.69	3.38	-17.82	-20.28	-8.27	5.37	-19.09	-21.90	-9.44	3.75	-18.81	-24.30	-18.42	5.43
	2A		-31.09	-41.55	-35.09	-	-33.08	-43.73	-35.72	-	-34.57	-43.72	-30.70	-	-34.50	-45.70	-37.54	-
	2A'		-29.24	-40.04	-36.25	-	-32.66	-43.37	-35.94	-	-32.79	-43.61	-36.28	-	-34.20	-44.72	-35.28	-
6-311++G(2d,p)	3	re	-18.03	-20.38	-7.88	2.40	-17.82	-19.71	-6.31	2.76	-15.71	-19.34	-12.17	4.58	-19.74	-21.41	-5.59	1.21
		si	-18.03	-20.38	-7.88	2.42	-17.82	-19.70	-6.32	2.46	-16.12	-19.31	-10.70	4.50	-19.74	-21.41	-5.59	1.42
	3'	re	-16.14	-18.17	-6.82	2.39	-17.56	-19.37	-6.05	2.55	-16.88	-18.71	-6.12	2.90	-14.24	-16.53	-7.68	2.75
		si	-16.14	-18.17	-6.82	2.38	-16.37	-18.84	-8.27	2.40	-17.52	-19.06	-5.14	2.66	-14.98	-17.38	-5.64	2.53
			Cl				OMe				NO_2				CN			
	1A		-23.42	-26.84	-11.48	3.40	-20.90	-24.37	-11.62	4.09	-26.37	-28.00	-5.44	3.37	-24.45	-28.84	-14.73	3.58
	1A'		-25.44	-28.86	-11.45	1.78	-23.02	-26.38	-11.27	3.38	-26.32	-27.87	-5.18	2.17	-25.37	-29.63	-14.29	1.56
	2A		-32.08	-43.59	-38.59	-	-35.59	-46.96	-38.14	-	-28.73	-39.57	-36.33	-	-30.28	-40.98	-35.86	-
	2A'		-30.55	-41.93	-38.17	-	-34.42	-45.76	-38.04	-	-29.41	-39.75	-34.68	-	-28.58	-40.18	-38.92	-
6-31+G(d,p)	3	re	-19.21	-20.58	-4.61	1.03	-19.93	-21.53	-5.37	1.42	-17.41	-19.73	-7.78	2.12	-18.04	-19.87	-6.14	1.74
		si	-19.21	-20.58	-4.60	1.03	-19.93	-21.53	-5.36	1.42	-17.41	-19.72	-7.77	4.95	-16.27	-20.72	-14.93	1.74
	3'	re	-18.28	-19.84	-5.22	1.56	-15.07	-17.30	-7.47	2.25	-20.95	-23.93	-10.00	2.55	-20.38	-22.03	-5.56	1.12
		si	-18.29	-19.84	-5.22	1.56	-16.86	-18.69	-6.16	2.25	-20.95	-23.93	-10.01	2.55	-20.16	-22.02	-6.25	1.12
	1A		-19.86	-24.72	-16.30	5.44	-18.81	-22.42	-12.12	4.71	-24.74	-26.25	-5.09	2.90	-22.38	-27.03	-15.62	4.20
	1A'		-21.81	-26.71	-16.45	3.45	-20.86	-24.38	-11.81	3.62	-24.88	-26.23	-4.51	1.88	-22.80	-27.62	-16.19	2.21
	2A		-29.14	-40.55	-38.26	-	-33.21	-43.89	-35.82	-	-25.40	-36.65	-37.73	-	-27.11	-37.92	-36.26	-
	2A'		-28.19	-39.32	-37.33	-	-31.63	-42.66	-37.01	-	-24.77	-36.69	-39.96	-	-26.50	-37.54	-37.02	-
6-311++G(2d,p)	3	re	-18.32	-19.82	-5.01	1.59	-18.66	-20.82	-7.24	2.21	-17.16	-19.01	-6.17	1.87	-16.92	-19.06	-7.19	2.56
		si	-18.32	-19.81	-5.01	1.61	-18.66	-20.82	-7.24	2.20	-17.17	-19.00	-6.17	1.86	-16.72	-19.44	-9.11	2.56
	3'	re	-16.82	-18.57	-5.87	2.53	-14.29	-16.73	-8.19	2.35	-21.38	-23.16	-5.95	1.12	-18.80	-21.11	-7.76	2.07
		si	-16.82	-18.57	-5.87	2.53	-15.98	-18.05	-6.95	2.36	-21.39	-23.16	-5.92	1.14	-18.80	-21.11	-7.76	2.08

[1] $kcal.mol^{-1}$
[2] $cal.mol^{-1}K^{-1}$

Mechanism A proceeds through two barrier energies for the nucleophilic addition (Fig. 5). The first transition state (TS) is an intermolecular TS, in which a C-N bond is formed, gradually. However, the second TS, as an intramolecular interaction, includes a C-O bond development. To have an insight into the most effective TS in reaction kinetics, the Energetic Span Model (ESM) was used [50-52].

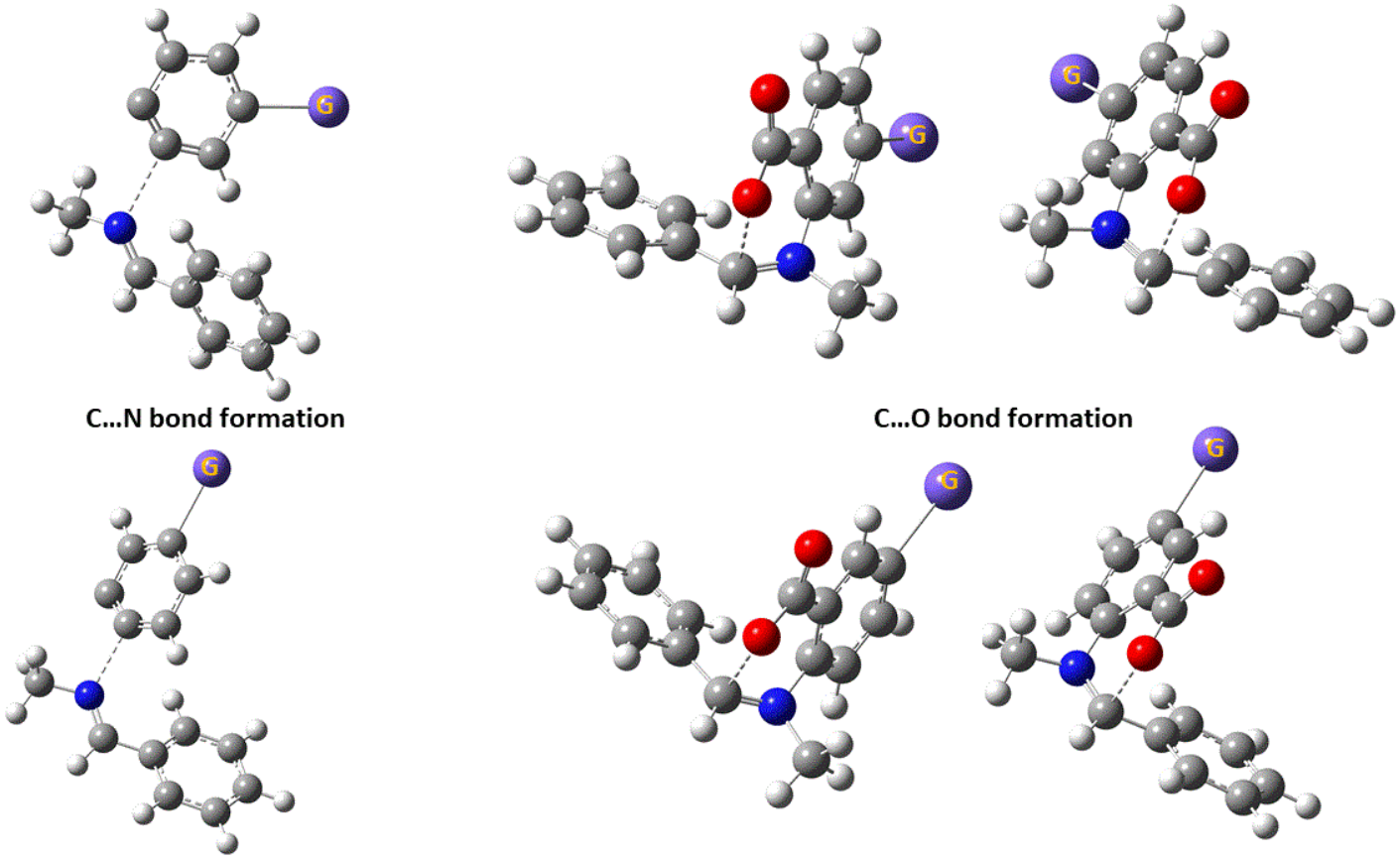

Fig. 5 C-N and C-O bond development during the reaction progress through TS1 and TS2 of mechanism A, respectively.

ESM is a powerful concept to describe the kinetic aspects of mechanism A. This model is applied to connect the energy profile acquired from the electronic-structure calculations to the turnover frequency (TOF) as an experimentally accessible quantity. TOF is described as the number of the productive cycles (N) per catalyst unit [Ct] and time (t) as illustrated in Eq (4) [53-56].

$$TOF = \frac{1}{[C_t]}\frac{dN}{dt} \qquad Eq(4)$$

ESM significantly allows the estimation of TOF of each considered route within determining the most effective TS and intermediate on the kinetic aspects of the reaction in the studied mechanism. Based on the Kozuch and Shaik report [53], TOF is evaluated by Eq (5).

$$TOF = \frac{k_B T}{h} . \frac{e^{-\Delta G_r/RT} - 1}{\sum_{i,j}^{N} e^{(T_i - I_j - \delta G'_{i,j})/RT}} \qquad Eq(5)$$

Where, ΔG_r is the overall reaction Gibbs energy, and T_i and I_j are the energies of the *ith* TS and the *jth* intermediate (In) in each step, respectively. k_B and h are the Boltzmann and Planck constants, respectively. R is the gas constant (1.98 cal $mol^{-1} \cdot K^{-1}$), and T is the absolute temperature (298.15 K). According to Eq (6), $\delta G'_{I,j}$ is equal to zero or ΔG_r.

$$\delta G'_{i,j} = \begin{cases} \Delta G_r & if\ i \geq j \\ 0 & if\ \ i < j \end{cases} \qquad Eq(6)$$

All the TSs and intermediates of a given reaction have not the same effect on the TOF of the reaction. Degree of TOF control (X_{TOF}) is used to specify the effect of each In and TS on the TOF in ESM to evaluate the TOF determining intermediate (TDI) and the TOF determining transition state (TDTS). Campbell's degree of rate control is a concept that develops the X_{TOF} [57,58], which measures the variation of TOF value by a small change in the TS or In energies. It can be calculated by Eq (7) [53].

$$X_{TOF,T_i} = \frac{\sum_j e^{(T_i - I_j - \delta G'_{i,j})/RT}}{\sum_{i,j} e^{\left(T_i - I_j - \delta G'_{i,j}\right)/RT}}$$

$$X_{TOF,I_j} = \frac{\sum_i e^{(T_i - I_j - \delta G'_{i,j})/RT}}{\sum_{i,j} e^{(T_i - I_j - \delta G'_{i,j})/RT}} \qquad Eq(7)$$

$$\sum_i X_{TOF,T_i} = 1 \qquad \sum_j X_{TOF,I_j} = 1$$

After that TDI and TDTS are evaluated, TOF equation (Eq (5)) can be abbreviated as Eq (8) in which, δE is the energetic span of the route.

$$TOF = \frac{k_B T}{h} . e^{-\delta E/RT} \qquad Eq(8)$$

$$\delta E = \begin{cases} T_{TDTS} - I_{TDI} & if\ TDTS\ occurs\ after\ TDI \quad (a) \\ T_{TDTS} - I_{TDI} + \Delta G_r & if\ TDTS\ occurs\ before\ TDI \quad (b) \end{cases}$$

Table 3 represents the X_{TOF} values for the involved TSs and intermediates for all steps of mechanism A and Fig. 6 depicts the Potential Energy Diagram (PED) for the reaction of Et-substituted aryne, as an example. Also, Fig. 7 depicts the involved species in the reaction. The obtained X_{TOF} values for the TS and intermediate of step1 are larger than others. Step1 plays a key role in the TOF of the reaction, which means that **In0** and **TS1** of both routes are TDI and TDTS of the reaction for all studied groups, respectively. Since TDTS occurs after TDI, δE is calculated by Eq (8-a). Table 4 shows the relative energy of the involved species, δE (kcal.mol^{-1}) and TOF (s^{-1}) values in which the summation of the absolute energies of aryne, CO_2 and imine molecules was considered as the energy reference.

The comparison of the barrier energies related to the C-N and C-O bond developments through the ESM reveals the greater effect of the C-N bond formation in the reaction kinetics. Thus the effect of the functional groups on the barrier energy of step 1, as the TDTS of the reaction, is more considerable than step 2. Two distinguishable trends are observed in the TDTS energy values. Generally, TDTS energies for electron- releasing groups are larger than that of electron-withdrawing ones. ELF is a powerful concept for explaining the observed TDTS energy trend of the substituted groups.

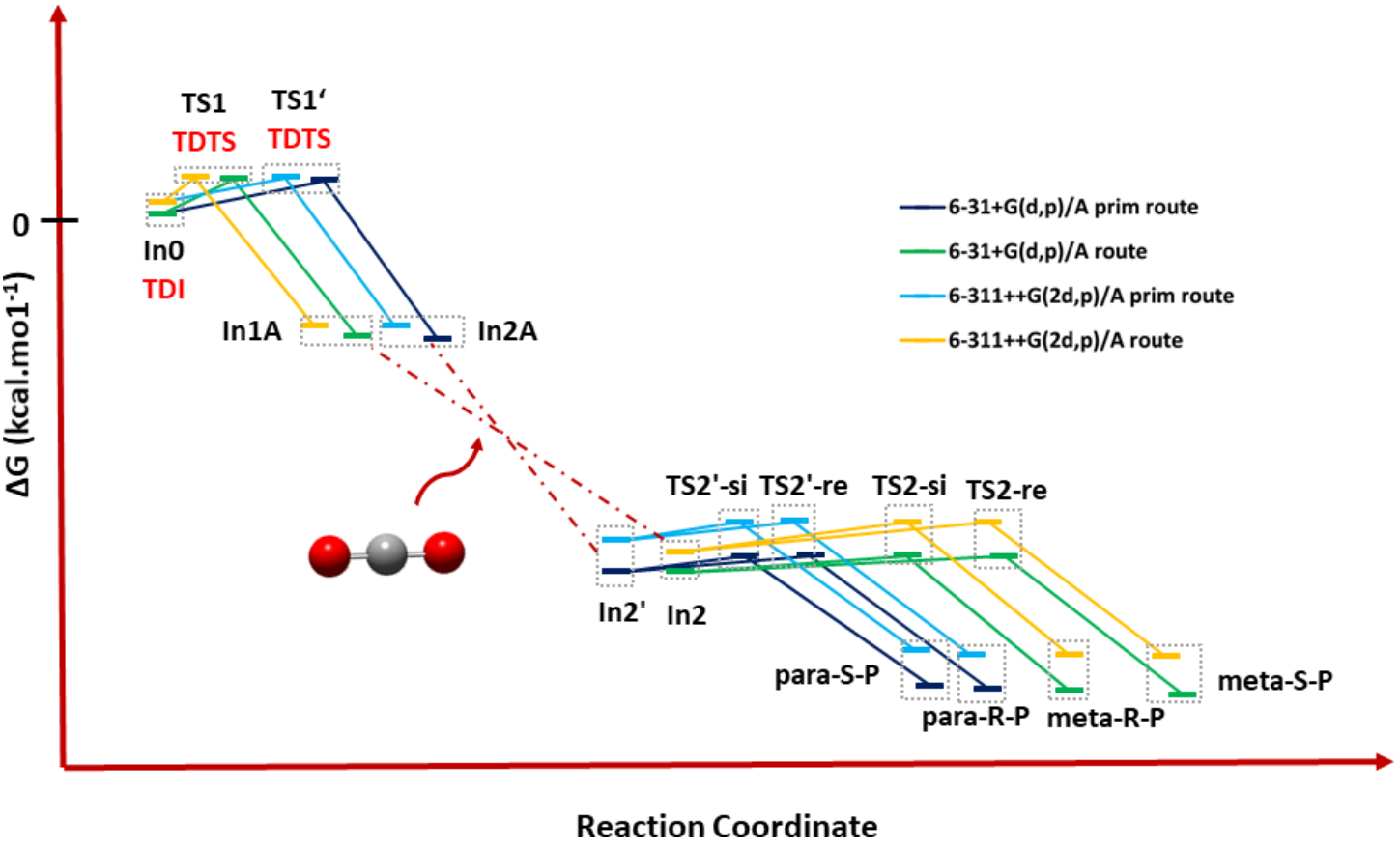

Fig. 6 Potential Energy Diagram (PED) for the reaction of Et-substituted aryne

Table 3 Degree of TOF control (X_{TOF}) of the possible reaction routes for all functional groups in both calculated levels

			Et				Me				Cl				NMe_2			
		Steps	In	$X_{TOF,Ij}$	TS	$X_{TOF,Ti}$	In	$X_{TOF,Ij}$	TS	$X_{TOF,Ti}$	In	$X_{TOF,Ij}$	TS	$X_{TOF,Ti}$	In	$X_{TOF,Ij}$	TS	$X_{TOF,Ti}$
6-31+G(d,p)	Route A	1A	In0	0.99	TS1	0.99	In0	1.00	TS1	1.00	In0	0.98	TS1	0.98	In0	0.99	TS1	0.99
		2A	In1A	0.00			In1A	0.00			In1A	0.00			In1A	0.00		
		3 re	In2	0.01	TS2-re / TS2-si	0.01	In2	0.00	TS2-re / TS2-si	0.00	In2	0.02	TS2-re / TS2-si	0.02	In2	0.01	TS2-re / TS2-si	0.01
		3 si																
	Route A'	1A'	In0	0.99	TS1'	0.99	In0	1.00	TS1'	1.00	In0	0.58	TS1'	0.58	In0	0.99	TS1'	0.99
		2A'	In2A	0.00			In2A	0.00			In2A	0.00			In2A	0.00		
		3' re	In2'	0.01	TS2'-re / TS2'-si	0.01	In2'	0.00	TS2'-re / TS2'-si	0.00	In2'	0.42	TS2'-re / TS2'-si	0.42	In2'	0.01	TS2'-re / TS2'-si	0.01
		3' si																
6-311++G(2d,p)	Route A	1A	In0	0.76	TS1	0.76	In0	0.96	TS1	0.96	In0	1.00	TS1	1.00	In0	0.99	TS1	0.99
		2A	In1A	0.00			In1A	0.00			In1A	0.00			In1A	0.00		
		3 re	In2	0.24	TS2-re / TS2-si	0.24	In2	0.04	TS2-re / TS2-si	0.04	In2	0.00	TS2-re / TS2-si	0.00	In2	0.01	TS2-re / TS2-si	0.01
		3 si																
	Route A'	1A'	In0	0.81	TS1'	0.81	In0	0.99	TS1'	0.99	In0	0.82	TS1'	0.82	In0	0.99	TS1'	0.99
		2A'	In2A	0.00			In2A	0.00			In2A	0.00			In2A	0.00		
		3' re	In2'	0.19	TS2'-re / TS2'-si	0.19	In2'	0.01	TS2'-re / TS2'-si	0.01	In2'	0.18	TS2'-re / TS2'-si	0.18	In2'	0.01	TS2'-re / TS2'-si	0.01
		3' si																
			F				CN				NO_2				OMe			
		Steps	In	$X_{TOF,Ij}$	TS	$X_{TOF,Ti}$	In	$X_{TOF,Ij}$	TS	$X_{TOF,Ti}$	In	$X_{TOF,Ij}$	TS	$X_{TOF,Ti}$	In	$X_{TOF,Ij}$	TS	$X_{TOF,Ti}$
6-31+G(d,p)	Route A	1A	In0	0.78	TS1	0.78	In0	0.99	TS1	0.99	In0	0.94	TS1	0.94	In0	0.99	TS1	0.99
		2A	In1A	0.00			In1A	0.00			In1A	0.00			In1A	0.00		
		3 re	In2	0.22	TS2-re / TS2-si	0.22	In2	0.01	TS2-re / TS2-si	0.01	In2	0.06	TS2-re / TS2-si	0.06	In2	0.01	TS2-re / TS2-si	0.01
		3 si																
	Route A'	1A'	In0	0.90	TS1'	0.90	In0	0.64	TS1'	0.64	In0	0.66	TS1'	0.66	In0	0.87	TS1'	0.87
		2A'	In2A	0.00			In2A	0.00			In2A	0.00			In2A	0.00		
		3' re	In2'	0.09	TS2'-re / TS2'-si	0.09	In2'	0.36	TS2'-re / TS2'-si	0.36	In2'	0.34	TS2'-re / TS2'-si	0.34	In2'	0.13	TS2'-re / TS2'-si	0.13
		3' si																
6-311++G(2d,p)	Route A	1A	In0	0.90	TS1	0.90	In0	0.94	TS1	0.94	In0	0.85	TS1	0.85	In0	0.99	TS1	0.99
		2A	In1A	0.00			In1A	0.00			In1A	0.00			In1A	0.00		
		3 re	In2	0.09	TS2-re / TS2-si	0.09	In2	0.06	TS2-re / TS2-si	0.06	In2	0.15	TS2-re / TS2-si	0.15	In2	0.01	TS2-re / TS2-si	0.01
		3 si																
	Route A'	1A'	In0	0.84	TS1'	0.84	In0	0.55	TS1'	0.55	In0	0.76	TS1'	0.76	In0	0.89	TS1'	0.89
		2A'	In2A	0.00			In2A	0.00			In2A	0.00			In2A	0.00		
		3' re	In2'	0.16	TS2'-re / TS2'-si	0.16	In2'	0.44	TS2'-re / TS2'-si	0.44	In2'	0.24	TS2'-re / TS2'-si	0.24	In2'	0.11	TS2'-re / TS2'-si	0.11
		3' si																

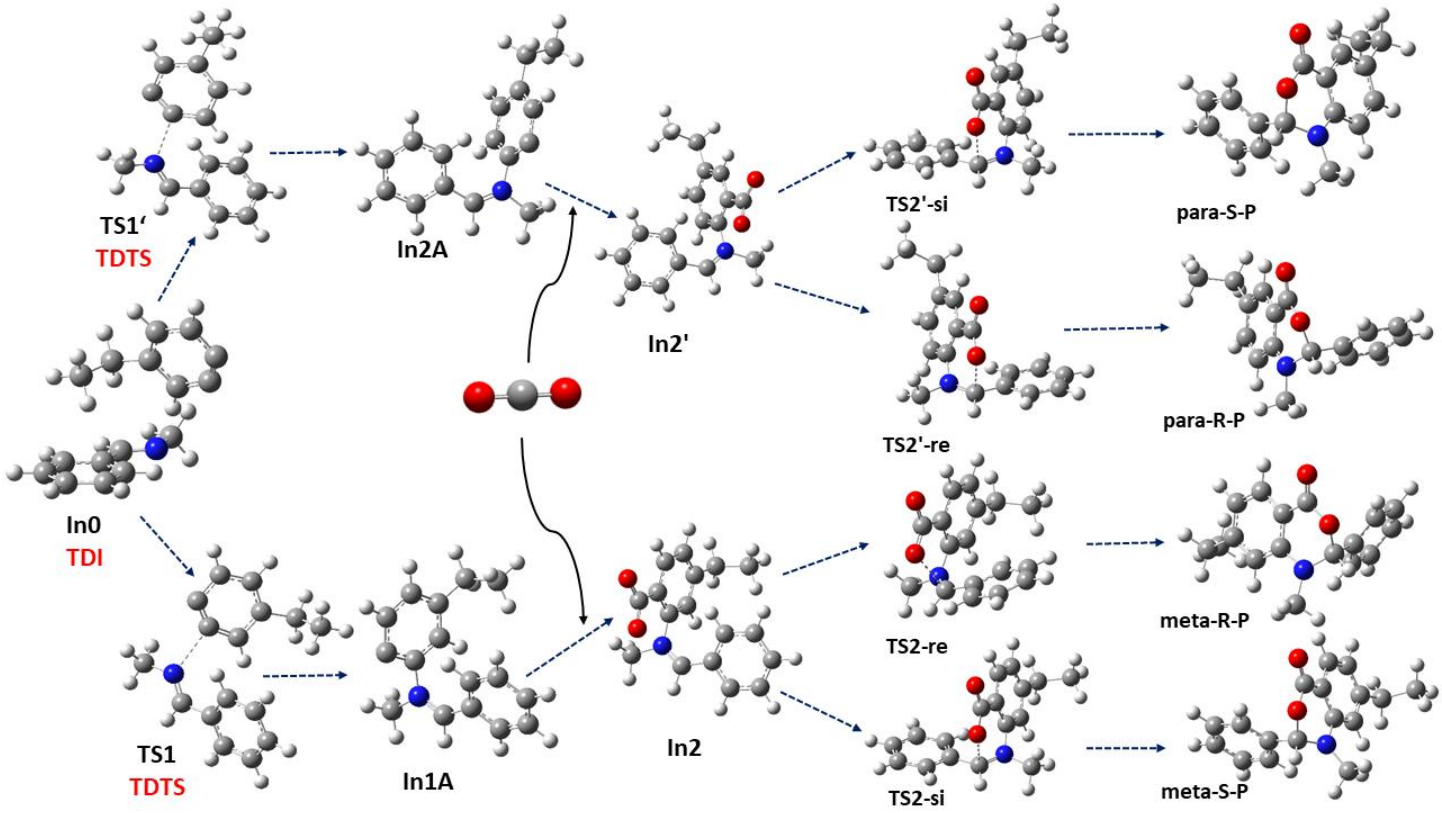

Fig. 7 Involved species in the reaction of Et-substituted aryne, as an example

Table 4 TDI, TDTS, δE (in kcal.mol^{-1}) and TOF (s^{-1}) values of the studied functional groups

		M06-2X/6-31+G(d,p)				M06-2X /6-311++G(2d,p)			
G	**Routes**	**TDI (kcal.mol^{-1})**	**TDTS (kcal.mol^{-1})**	**δE (kcal.mol^{-1})**	**TOF (s^{-1})**	**TDI (kcal.mol^{-1})**	**TDTS (kcal.mol^{-1})**	**δE (kcal.mol^{-1})**	**TOF (s^{-1})**
Et	A	5.77	11.19	5.43	6.5×10^{8}	7.61	11.42	4.50	2.4×10^{9}
	A'	5.77	10.96	5.19	9.7×10^{8}	7.61	11.36	3.75	8.9×10^{9}
Cl	A	6.76	10.16	3.40	2.0×10^{10}	5.01	10.44	5.44	6.4×10^{8}
	A'	6.76	8.55	1.78	1.8×10^{11}	5.01	8.46	3.45	1.5×10^{10}
F	A	6.47	9.73	3.26	2.0×10^{10}	6.01	10.16	4.15	5.1×10^{9}
	A'	6.47	9.73	3.26	2.3×10^{10}	6.01	9.39	3.38	1.7×10^{10}
Me	A	5.51	10.16	4.65	2.4×10^{9}	6.04	10.32	4.28	4.3×10^{9}
	A'	5.51	10.59	5.08	1.2×10^{9}	6.04	11.41	5.37	7.1×10^{8}
NMe_2	A	6.59	10.56	3.97	7.6×10^{9}	6.28	10.73	4.46	3.3×10^{9}
	A'	6.59	11.46	4.88	1.6×10^{9}	6.28	11.71	5.43	6.4×10^{8}
CN	A	6.46	10.04	3.58	1.4×10^{10}	6.00	10.20	4.20	4.9×10^{9}
	A'	6.46	8.01	1.56	2.9×10^{11}	6.00	8.22	2.21	8.2×10^{10}
NO_2	A	5.47	7.65	4.95	1.4×10^{9}	5.86	8.76	2.90	3.9×10^{10}
	A'	5.47	8.84	2.55	5.4×10^{10}	5.86	7.75	1.88	2.0×10^{11}
OMe	A	6.69	10.78	4.09	6.2×10^{9}	6.48	11.18	4.71	2.2×10^{9}
	A'	6.69	10.07	3.38	1.8×10^{10}	6.48	10.09	3.62	1.2×10^{10}

ELF analysis is another molecular descriptor, which can be applied for justification of the nucleophilic attack of the imine to the substituted arynes [59-61]. ELF analysis generates basin spaces, in which the probability of electron pair existence in these spaces is maximal. Generally, the basins are divided into core and valence kinds. The latter is specified by the synaptic order, i.e., the number of atomic valence shells that they participate [62]. Therefore, three main monosynaptic, disynaptic, and trisynaptic basins are distinguishable. A monosynaptic basin, V(A), related to a lone pair or non-bonding regions on atom A, V(A,B) as a disynaptic basin refers to the core of two nuclei of A and B, which describes a bonding region between A and B. A trisynaptic basin, V(A,B,C), corresponds to a three-center bond and so on. ELF concept is similar to the Lewis bonding model that provides a graphical representation of the molecular system. Based on this concept, two monosynaptic basins, $V(C_x)$ and $V(C_y)$ are merged into a new disynaptic basin $V(C_x,C_y)$, corresponding to the formation of the new single C_x–C_y bond [63,64].

Based on the ELF terminology, involved basins in the reaction for the substituted arynes are disynaptic basins C2-C3 ($V(C_2,C_3)$), C3-C4 ($V(C_3,C_4)$) and C4-C5 ($V(C_4,C_5)$) bonds. Also, the nitrogen atom of the imine compound has a monosynaptic basin, V(N). In TS1 and TS1', the electron density of V(N) basin decreases and the disynaptic basin (V(C,N)) corresponding to the C-N bond is developed, gradually. Fig. 8 and Table 5 represent the involved basins in the reaction and their calculated electron density for steps 1A and 1A', respectively

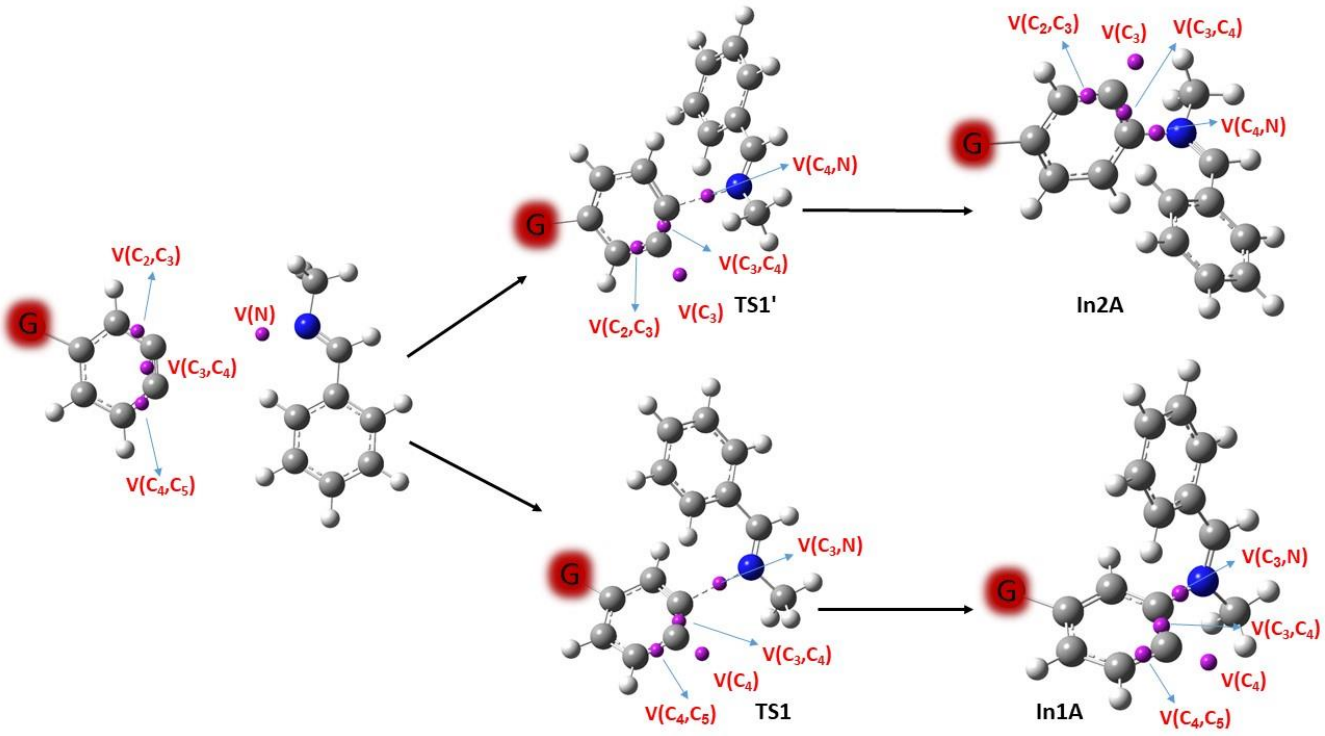

Fig. 8 The position of the participating basins in the first steps of both routes in mechanism A

Table 5 Calculated electron density (a.u) of the involved basins in steps 1A and 1A'

			NO_2	CN	F	Cl	OMe	Me	Et	NMe_2
6-31+G(d,p)	Aryne	$V(C_2,C_3)$	2.7849	2.7469	2.7075	2.7676	3.4018	3.4513	3.4560	3.4092
		$V(C_3,C_4)$	3.3648	3.3684	3.3933	3.3819	3.4141	3.3624	3.3602	3.3643
		$V(C_4,C_5)$	3.3855	3.3839	3.4323	3.4292	3.4502	3.4975	3.4991	3.5682
	TS1	$V(C_4)$	1.3116	1.4341	1.5360	1.5460	1.7008	1.6935	1.7053	1.7803
		$V(C_3,C_4)$	3.4684	3.4496	3.4968	3.4595	3.5099	3.4216	3.4016	3.4389
		$V(C_4,C_5)$	2.3613	2.3167	2.2966	2.2871	2.1907	2.2155	2.2262	2.1816
		$\Delta V(C_4,C_5)$	1.0242	1.0672	1.1357	1.1421	1.2595	1.2820	1.2729	1.3866
	TS1'	$V(C_3)$	1.4738	1.4146	1.4962	1.4853	1.5561	1.6289	1.6514	1.6109
		$V(C_3,C_4)$	3.4360	3.4529	3.4429	3.4403	3.4444	3.4175	3.4008	3.3780
		$V(C_2,C_3)$	2.5742	2.3978	2.3149	2.3366	2.2476	2.2483	2.2333	2.2889
		$\Delta V(C_2,C_3)$	0.2108	0.3491	0.3926	0.4310	1.1542	1.2030	1.2227	1.1203
	In1A	$V(C_3,N)$	1.9485	1.9484	1.9579	1.9571	1.9724	1.9703	1.9709	1.9791
		$V(C_4)$	2.3257	2.3276	2.3749	2.3580	2.3937	2.3781	2.3712	2.4148
	In2A	$V(C_4,N)$	1.9452	1.9464	1.9616	1.9550	1.9681	1.9595	1.9599	1.9770
		$V(C_3)$	2.3499	2.3468	2.3408	2.3419	2.3450	2.3625	2.3654	2.3424
6-311++G(2d,p)	Aryne	$V(C_2,C_3)$	2.8741	2.8343	3.3633	3.3903	3.2516	3.3055	3.3061	3.2403
		$V(C_3,C_4)$	3.6646	3.6652	3.7287	3.6922	3.7394	3.6583	3.6502	3.6989
		$V(C_4,C_5)$	3.2355	3.2362	3.2516	3.2722	3.3121	3.3668	3.3744	3.4371
	TS1	$V(C_4)$	1.2218	1.3636	1.4638	1.4716	1.6402	1.6396	1.6562	1.7170
		$V(C_3,C_4)$	3.6330	3.5792	3.6157	3.5888	3.6072	3.5354	3.5124	3.5317
		$V(C_4,C_5)$	2.4091	2.3611	2.3334	2.3243	2.2203	2.2399	2.2505	2.2127
		$\Delta V(C_4,C_5)$	0.8265	0.8751	0.9182	0.9479	1.0918	1.1269	1.1240	1.2244
	TS1'	$V(C_3)$	1.3532	1.3327	1.4363	1.4384	1.4989	1.5602	1.5823	1.5538
		$V(C_3,C_4)$	3.7114	3.5901	3.5838	3.5806	3.6017	3.5400	3.5302	3.5278
		$V(C_2,C_3)$	2.6358	2.4313	2.3518	2.3590	2.2879	2.2786	2.2712	2.3289
		$\Delta V(C_2,C_3)$	0.2383	0.4031	1.0115	1.0314	0.9637	1.0269	1.0349	0.9114
	In1A	$V(C_3,N)$	1.9984	1.9979	2.0002	2.0021	2.0132	2.0158	2.0088	2.0075
		$V(C_4)$	2.3259	2.3325	2.3724	2.3522	2.3916	2.3746	2.3699	2.4077
	In2A	$V(C_4,N)$	1.9920	2.0014	2.0037	2.0000	2.0184	2.2893	2.0159	2.0155
		$V(C_3)$	2.3477	2.3471	2.3417	2.3424	2.3435	2.3577	2.3588	2.3469

The reaction progress from the reactants to the TS1 and TS1' is followed by decreasing the electron density of $V(C_4,C_5)$ and $V(C_2,C_3)$ basins and increasing that for $V(C_3,C_4)$ basin. Also, monosynaptic basins $V(C_4)$ and $V(C_3)$ corresponding to TS1 and TS1' are developed on the related carbon atoms, respectively. In the case of TS1', a good linear correlation can be seen between $\Delta G^{\neq}$ values of TDSTs and the electron density of monosynaptic basin $V(C_3)$. However, in TS1, the correlation for $V(C_4)$ electron density values is not acceptable (Fig. 9). The difference between the electron densities of $V(C_4,C_5)$ basins in arynes and TS1($\Delta V(C_4,C_5)$) is greater than that of $V(C_2,C_3)$ basin in arynes and TS1' ($\Delta V(C_2,C_3)$). As a result, in comparison to the nucleophilic addition of the imine

to C4 in TS1', the addition to C3 atom in TS1 causes a larger decline in the electron densities of V(C_4,C_5) basins, making a significant electron density development for V(C_4) basin. This addition to C4 atom results in a lower electron density growth for V(C_3) basin.

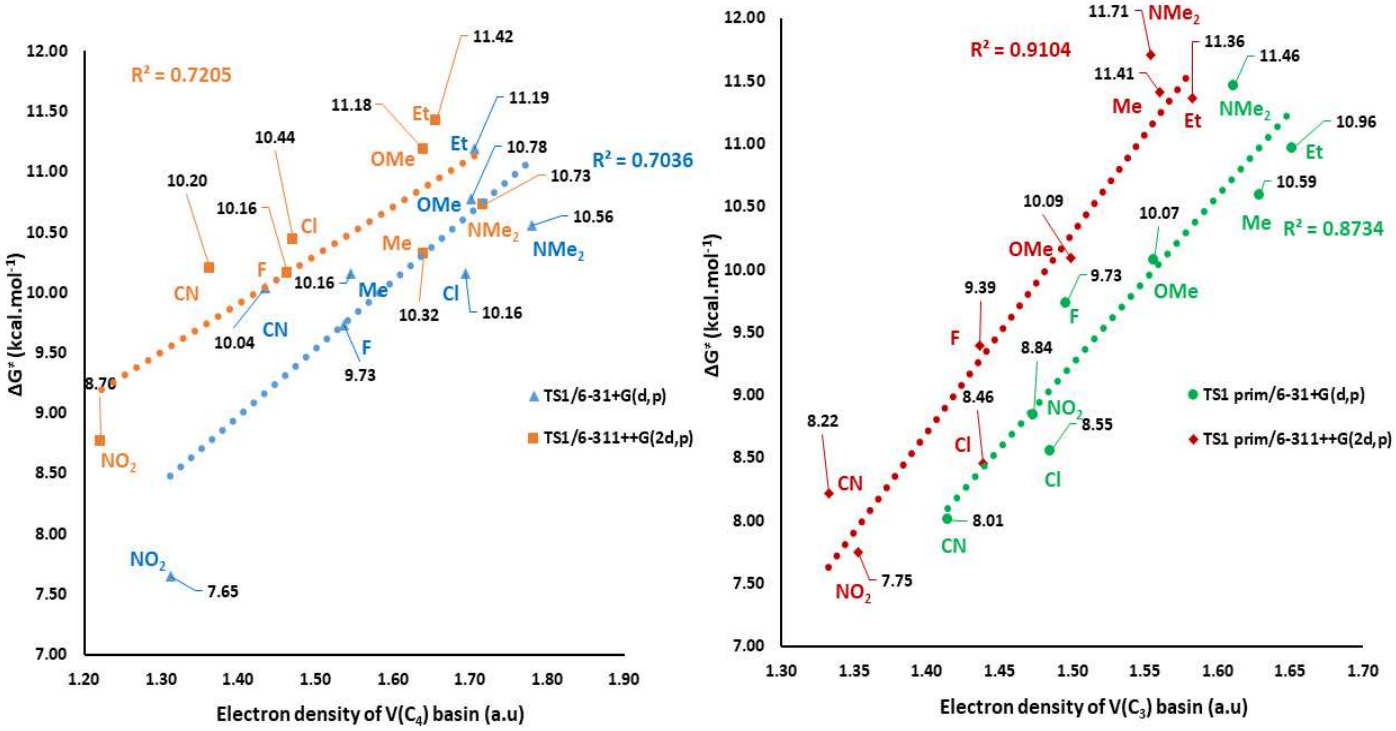

Fig. 9 Linear correlation between the electron density of V(C_4) and V(C_3) basins and $\Delta G^{\neq}$ of TDSTs

ELF analysis is followed by an evaluation of the electron density of the C1-G basin, in which G and C1 are the bonded atoms of the substituents to the aryne ring and carbon atom of the ring, respectively. Fig. 9 depicts the electron density contributions of the C1 and G atoms in the total electron density of C1-G basins (V(C_1,G)) for both TS1 and TS1'. The obtained results show that in the nucleophilic addition to C3 atom (TS1), the contribution of C1 in electron density of V(C_1,G) is greater than that of in the addition to C4 atom (TS1'). Also, the developed natural charge on the C4 atom in TS1 is more significant than the C3 natural charge in TS1'(Fig. 10). This can be related to the larger electron density of V(C_4,C_5) basins decreasing along the TS1 than that of V(C_2,C_3) basins in the TS1'. On the other hand, C4 and C3 atoms are in para and meta positions relative to substituted groups in TS1and TS1', respectively. It seems that more effective interaction of developing electron density on C4 atom in para position with the substituted groups (G) causes further natural charge growth on this atom, indeed the substituted groups have more significant effects on the electron density of C4 atoms at TS1. These effects can be considered as a mixture of inductive and resonance effects. The poor linear correlation between $\Delta G^{\neq}$ values of the TDSTs and electron densities of V(C_4) basin may be owning to these different effects

of the substituents on the C4 position. Finally, in the case of In1A and In2A, the electron density of V(C_3,N) basins is somewhat greater than V(C_4,N).

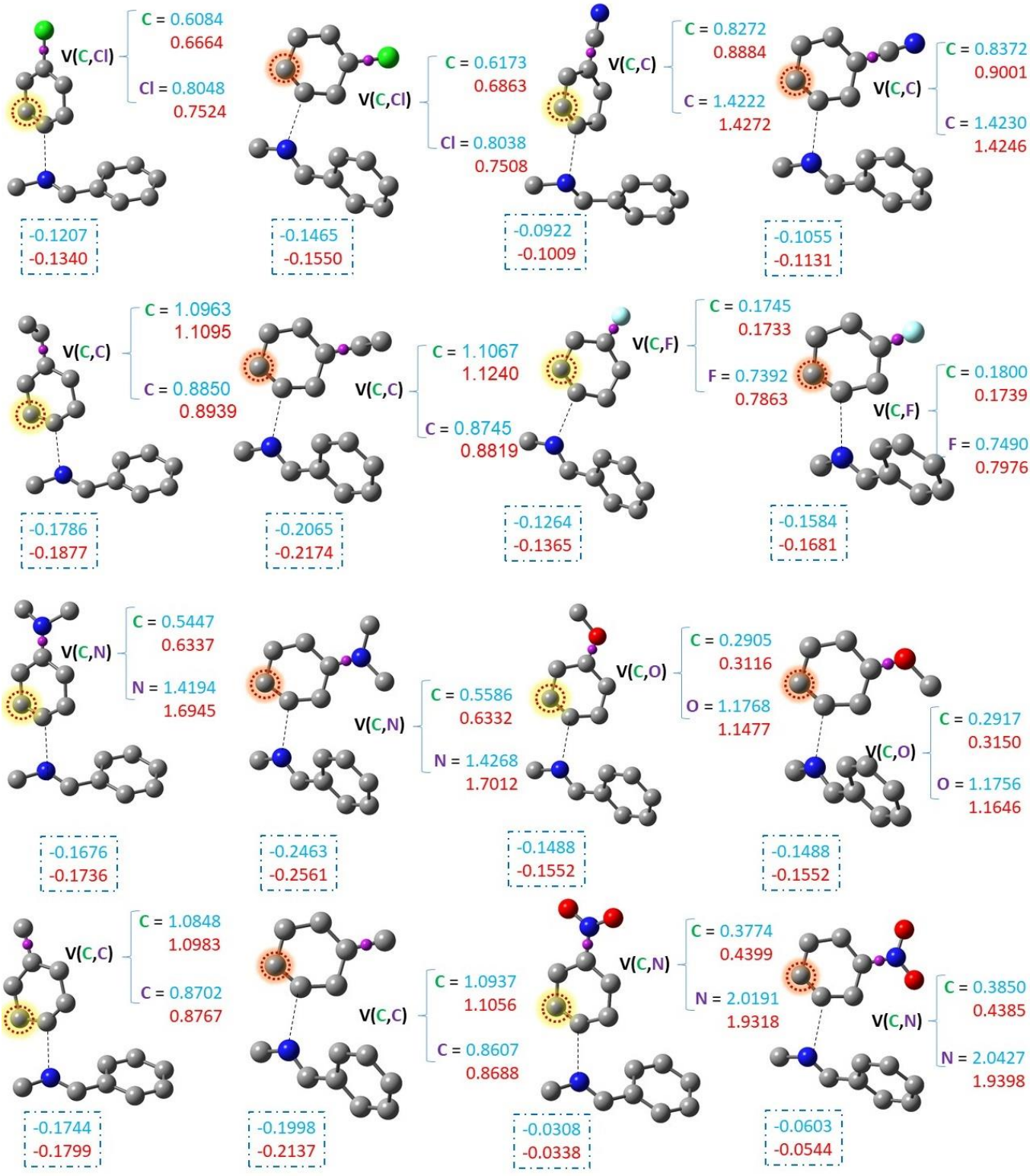

Fig. 10 The electron density contributions (in a.u) of C1(in green color) and G (in purple color) atoms in V(C_1,G) basins for both TS1 and TS1' and developed natural charges on C3 and C4 atoms at 6-31+G(d,p) (Blue color) and 6-311++G(2d,p) (Red color) levels (Hydrogen atoms have been omitted for more clarity)

Conclusion

Benzoxazinone formation by CO_2 incorporation can proceed through two mechanisms. In mechanism A, which is initiated by addition to the substituted arynes, the imine compound behaves as the nucleophile, while, in mechanism B the reaction is started by the nucleophilic addition of arynes to CO_2. The calculated results at M06-2X/6-31+G(d,p) and M06-2X/6-311++G(2d,p) levels showed that mechanism B proceeds within the large values of activation barrier energy in the first step. Generally, four stereoisomers can be considered for the final product. The results of X_{TOF} analyses in ESM reveal that TS1 and TS1' are TDTS of routes A and A', respectively. Also, In0 is considered as the TDI for both routes. ELF analysis was used to investigate the calculated TDTS energy trends. The reaction in step1 and 1' is followed by the electron densities of V(C_4) and V(C_3) basin development corresponding to the TS1 and TS1', respectively, which accomplishes by decreasing the electron density of V(C_4,C_5) and V(C_2,C_3) basins and increasing that for V(C_3,C_4) basin in TS1 and TS1', respectively. Therefore, the variation of V(C_4,C_5) and V(C_2,C_3) along with the reaction progress from the substituted arynes to the TSs has a remarkable effect on the electron densities of V(C4) and V(C3) basins. A good linear correlation can be seen between the TDTS energy values and V(C_3) electron densities. Nonetheless, this correlation was not considered for TS1. Furthermore, the greater contribution of C1 atom of arynes in the electron density of V(C_1,G) basin at TS1 than TS1' was another consequence of ELF analysis, which reveals that the interactions of the substituents groups and aryne ring in TS1 and TS1' are different, significantly.

Acknowledgments We hereby acknowledge that some parts of this computation were performed in the HPC center of the Ferdowsi University of Mashhad.

Author contributions Hossein Sabet-Sarvestani devised the project, the main conceptual ideas and wrote the first draft of the manuscript, Hossein Eshghi rewrote the manuscript and Mohammad Izadyar supervised and edited the manuscript and approved the final version.

Funding Research Council of the Ferdowsi University of Mashhad is gratefully acknowledged for the financial support of this project (Grant No2/51154).

Availability of data and material The authors confirm that the data supporting the findings of this study are available within the supporting information as a separated word file includes Tables and Cartesian coordinates of the molecules.

Compliance with ethical standards

Conflict of interest The authors declare no conflict of interest.

Ethical approval This article does not contain any studies with human participants or animals performed by any of the authors.

References

1. Bryden TS, Hilton G, Cruden A, Holton T (2018) Electric vehicle fast charging station usage and power requirements. Energy 152:322-332
2. Song C (2006) Global challenges and strategies for control, conversion and utilization of CO_2 for sustainable development involving energy, catalysis, adsorption and chemical processing. Catal today 115:2-32
3. Song Q-W, Zhou Z-H, He L-N (2017) Efficient, selective and sustainable catalysis of carbon dioxide. Green Chem 19:3707-3728
4. Zhu Q (2019) Developments on CO_2-utilization technologies. Clean Energy 3:85-100
5. Ghara M, Chattaraj PK (2019) A computational study on hydrogenation of CO_2, catalyzed by a bridged B/N frustrated Lewis pair. Struct Chem 30:1067-1077
6. Correa A, Leon T, Martin R (2014) Ni-catalyzed carboxylation of C (sp^2)–and C (sp^3)–O bonds with CO_2. J Am Chem Soc 136:1062-1069
7. Qin H-L, Han J-B, Hao J-H, Kantchev EAB (2014) Computational and experimental comparison of diphosphane and diene ligands in the Rh-catalysed carboxylation of organoboron compounds with CO_2. Green Chem 16:3224-3229
8. Finn C, Schnittger S, Yellowlees LJ, Love JB (2012) Molecular approaches to the electrochemical reduction of carbon dioxide. Chem Commun 48:1392-1399
9. Sabet-Sarvestani H, Izadyar M, Eshghi H (2020) Evaluation and understanding the performances of various derivatives of carbonyl-stabilized Phosphonium ylides in CO_2 transformation to cyclic carbonates. Phys Chem Chem Phys 22:223-237
10. Kamphuis AJ, Picchioni F, Pescarmona PP (2019) CO_2-fixation into cyclic and polymeric carbonates: principles and applications. Green Chem 21:406-448
11. Ma J, Liu J, Zhang Z, Han B (2012) The catalytic mechanism of KI and the co-catalytic mechanism of hydroxyl substances for cycloaddition of CO_2 with propylene oxide. Green Chem 14:2410-2420
12. Klaus S, Lehenmeier MW, Anderson CE, Rieger B (2011) Recent advances in CO_2/epoxide copolymerization—new strategies and cooperative mechanisms. Coord Chem Rev 255:1460-1479
13. Lu X-B, Ren W-M, Wu G-P (2012) CO_2 copolymers from epoxides: catalyst activity, product selectivity, and stereochemistry control. Acc Chem Res 45:1721-1735
14. von der Assen N, Bardow A (2014) Life cycle assessment of polyols for polyurethane production using CO_2 as feedstock: insights from an industrial case study. Green Chem 16:3272-3280
15. Kimura T, Kamata K, Mizuno N (2012) A bifunctional tungstate catalyst for chemical fixation of CO_2 at atmospheric pressure. Angew Chem Int Ed 51:6700-6703
16. Kee CW, Peh KQE, Wong MW (2017) Coupling Reactions of Alkynyl Indoles and CO_2 by Bicyclic Guanidine: Origin of Catalytic Activity? Chem Asian J 12:1780-1789
17. Zhu L, Ye J-H, Duan M, Qi X, Yu D-G, Bai R, Lan Y (2018) The mechanism of copper-catalyzed oxytrifluoromethylation of allylamines with CO_2: a computational study. Org Chem Front 5:633-639
18. Alkorta I, Elguero J (2019) Prototropic tautomerism of the addition products of N-heterocyclic carbenes to CO_2, CS_2, and COS. Struct Chem 30:1971-1979
19. Sabet-Sarvestani H, Eshghi H, Izadyar M (2017) A theoretical study on the efficiency and role of guanidines-based organic superbases on carbon dioxide utilization in quinazoline-2, 4 (1H, 3H)-diones synthesis. Struct Chem 28:675-686
20. Brinckerhoff P (2011) Accelerating the uptake of CCS: industrial use of captured carbon dioxide. Global CCS Institute 260
21. Chen F, Li M, Wang J, Dai B, Liu N (2018) Fe (II) complexes: reservoirs for Lewis acids and carbenes and their utility in the conversion of CO_2 to oxazolidinones. J CO_2 Util 28:181-188
22. Marchegiani M, Nodari M, Tansini F, Massera C, Mancuso R, Gabriele B, Costa M, Della Ca N (2017) Urea derivatives from carbon dioxide and amines by guanidine catalysis: Easy access to imidazolidin-2-ones under solvent-free conditions. J CO_2 Util 21:553-561

23. Zhu A, Tang M, Lv Q, Li L, Bai S, Li Q, Feng W, Li Q, Wang J (2019) Fixation of CO_2 in structurally diverse quinazoline-2, 4 (1H, 3H)-diones under ambient conditions. J CO_2 Util 34:500-506
24. Lang X-D, Yu Y-C, Li Z-M, He L-N (2016) Protic ionic liquids-promoted efficient synthesis of quinazolines from 2-aminobenzonitriles and CO_2 at ambient conditions. J CO_2 Util 15:115-122
25. Vessally E, Soleimani-Amiri S, Hosseinian A, Edjlali L, Babazadeh M (2017) Chemical fixation of CO_2 to 2-aminobenzonitriles: A straightforward route to quinazoline-2, 4 (1H, 3H)-diones with green and sustainable chemistry perspectives. J CO_2 Util 21:342-352
26. Candeias NR, Branco LC, Gois PM, Afonso CA, Trindade AF (2009) More sustainable approaches for the synthesis of N-based heterocycles. Chem Rev 109:2703-2802
27. Wu X-F, Neumann H, Beller M (2012) Synthesis of heterocycles via palladium-catalyzed carbonylations. Chem Rev 113:1-35
28. Yuan J, Liu C, Lei A (2015) Construction of N-containing heterocycles via oxidative intramolecular N–H/X–H coupling. Chem Commun 51:1394-1409
29. Noel S, Cadet S, Gras E, Hureau C (2013) The benzazole scaffold: a SWAT to combat Alzheimer's disease. Chem Soc Rev 42:7747-7762
30. Prajapati NP, Vekariya RH, Borad MA, Patel HD (2014) Recent advances in the synthesis of 2-substituted benzothiazoles: a review. RSC Adv 4:60176-60208
31. Shi X, Guo J, Liu J, Ye M, Xu Q (2015) Unexpectedly Simple Synthesis of Benzazoles by tBuONa-Catalyzed Direct Aerobic Oxidative Cyclocondensation of o-Thio/Hydroxy/Aminoanilines with Alcohols under Air. Chem–A Eur J 21:9988-9993
32. Shariat M, Abdollahi S (2004) Synthesis of benzoxazinone derivatives: a new route to 2 (N Phthaloylmethyl)-4H-3, 1-benzoxazin-4-one. Molecules 9:705-712
33. Wang S, Xi C (2019) Recent advances in nucleophile-triggered CO_2-incorporated cyclization leading to heterocycles. Chem Soc Rev 48:382-404
34. Yoshida H, Fukushima H, Ohshita J, Kunai A (2006) CO_2 incorporation reaction using arynes: Straightforward access to benzoxazinone. J Am Chem Soc 128:11040-11041
35. Sabet-Sarvestani H, Izadyar M, Eshghi H, Noroozi-Shad N, Bakavoli M (2018) Proton sponge as a new efficient catalyst for carbon dioxide transformation to methanol: Theoretical approach. Fuel 221:491-500
36. Sabet-Sarvestani H, Izadyar M, Eshghi H, Noroozi-Shad N (2018) Understanding the thermodynamic and kinetic performances of the substituted phosphorus ylides as a new class of compounds in carbon dioxide activation. Energy 145:329-337
37. Sabet-Sarvestani H, Izadyar M, Eshghi H (2017) Phosphorus ylides as a new class of compounds in CO_2 activation: Thermodynamic and kinetic studies. J CO_2 Util 21:459-466
38. Sabet-Sarvestani H, Eshghi H, Izadyar M (2017) Understanding the mechanism, thermodynamic and kinetic features of the Kukhtin–Ramirez reaction in carbamate synthesis from carbon dioxide. RSC Adv 7:1701-1710
39. Rakhshanipour M, Sabet-Sarvestani H, Eshghi H (2020) Performance studies of CO_2 transformation to methanol by zwitterionic indenylammonium derivatives as a new class of carbon-centered organocatalysts. Struct Chem 31:585-598
40. Sabet-Sarvestani H, Eshghi H (2021) Theoretical introduction and design of Si/N catalysts as efficient reducing agents in CO_2 hydroboration by planar Si/N π-conjugated molecules. Struct Chem doi.org/10.1007/s11224-020-01704-8
41. Zhao Y, Truhlar DG (2008) The M06 suite of density functionals for main group thermochemistry, thermochemical kinetics, noncovalent interactions, excited states, and transition elements: two new functionals and systematic testing of four M06-class functionals and 12 other functionals. Theor Chem Acc 120:215-241
42. Frisch M, Trucks G, Schlegel H, Scuseria G, Robb M, Cheeseman J, Scalmani G, Barone V, Mennucci B, Petersson G, Nakatsuji H, Caricato M, Li X, Hratchian HP, Izmaylov AF, Bloino J, Zheng G, Sonnenberg JL, Hada M, Ehara M, Toyota K, Fukuda R, Hasegawa J, Ishida M, Nakajima T, Honda Y, Kitao O, Nakai H, Vreven T, Montgomery JA, Jr, Peralta JE, Ogliaro F, Bearpark M, Heyd JJ, Brothers E, Kudin KN, Staroverov VN, Kobayashi R, Normand J, Raghavachari K, Rendell A, Burant JC, Iyengar SS, Tomasi J, Cossi M, Rega N, Millam JM, Klene M, Knox JE, Cross JB, Bakken V, Adamo C, Jaramillo J, Gomperts R, Stratmann RE, Yazyev O, Austin AJ, Cammi R, Pomelli C, Ochterski JW, Martin RL, Morokuma K, Zakrzewski VG, Voth GA, Salvador P, Dannenberg JJ, Dapprich S, Daniels AD, Farkas O, Foresman JB, Ortiz JV, Cioslowski J, Fox DJ (2009) Gaussian 09, revision A. 1; Gaussian, Inc: Wallingford, CT.
43. Kóňa J, Fabian WM (2011) Hybrid QM/MM Calculations on the First Redox Step of the Catalytic Cycle of Bovine Glutathione Peroxidase GPX1. J Chem Theory Comput 7 (8):2610-2616

44. Becke AD (1993) Density-functional thermochemistry. III. The role of exact exchange. J Chem Phys 98:5648-5652
45. Fukui K (1970) Formulation of the reaction coordinate. J Phys Chem 74:4161-4163
46. Heverly-Coulson GS, Boyd RJ (2010) Theoretical investigations on the reaction of monosubstituted tertiary-benzylamine selenols with hydrogen peroxide. J Phys Chem A 114:10706-10711
47. Lu T, Chen F (2012) Multiwfn: a multifunctional wavefunction analyzer. J Comput Chem 33:580-592
48. Carey FA, Sundberg RJ (2007) Advanced Organic Chemistry: Part A: Structure and Mechanisms. Springer Science & Business Media
49. Domingo LR, Pérez P, Sáez JA (2013) Understanding the local reactivity in polar organic reactions through electrophilic and nucleophilic Parr functions. RSC Adv 3:1486-1494
50. Hao Z, Guo L, Xing M, Zhang Q (2019) Mechanistic study of ethanol steam reforming on TM–Mo_6S_8 clusters: a DFT study. Catal Sci Technol 9:1631-1643
51. Guo L, Cao Z, Liu N, An X, Li A, Li W, Zheng X (2016) Mechanisms of the water–gas shift reaction catalyzed by carbonyl complexes $M(CO)_6$ (M= Mo, W). Int J Hydrog Energy 41:2432-2446
52. Ma L-L, Wang W, Wang G-C (2016) Theoretical investigations toward the [3+ 2]-dipolar cycloadditions of nitrones with vinyldiazoacetates catalyzed by Rh_2(R-TPCP)$_4$: mechanism and enantioselectivity. RSC Adv 6:53839-53851
53. Kozuch S, Shaik S (2010) How to conceptualize catalytic cycles? The energetic span model. Acc Chem Res 44:101-110
54. Kheirabadi R, Izadyar M, Housaindokht MR (2017) Computational Kinetic Modeling of the Catalytic Cycle of Glutathione Peroxidase Nanomimic: Effect of Nucleophilicity of Thiols on the Catalytic Activity. J Phys Chem A 122:364-374
55. Falivene L, Kozlov SM, Cavallo L (2018) Constructing Bridges between Computational Tools in Heterogeneous and Homogeneous Catalysis. ACS Catal 8:5637-5656
56. Zhang Y-w, Wang Y-C, Zhang X-j, Wang X-l, Li S (2018) A theoretical study on La-activated bicyclo-oligomerization of acetylene to form naphthalene in gas phase using density functional theory (DFT). Struct Chem 29:171-178
57. Campbell CT (2001) Finding the rate-determining step in a mechanism: comparing dedonder relations with the “Degree of Rate Control”. Elsevier
58. Stegelmann C, Andreasen A, Campbell CT (2009) Degree of rate control: How much the energies of intermediates and transition states control rates. J Am Chem Soc 131:8077-8082
59. Polo V, Andres J, Berski S, Domingo LR, Silvi B (2008) Understanding reaction mechanisms in organic chemistry from catastrophe theory applied to the electron localization function topology. J Phys Chem A 112:7128-7136
60. Andres J, Berski S, R Domingo L, Polo V, Silvi B (2011) Describing the molecular mechanism of organic reactions by using topological analysis of electronic localization function. Curr Org Chem 15:3566-3575
61. Andrés J, Berski S, Domingo LR, González-Navarrete P (2012) Nature of the ring-closure process along the rearrangement of octa-1, 3, 5, 7-tetraene to cycloocta-1, 3, 5-triene from the perspective of the electron localization function and catastrophe theory. J Comput Chem 33 (7):748-756
62. Silvi B (2002) The synaptic order: a key concept to understand multicenter bonding. J Mol Struct 614:3-10
63. R Domingo L, Chamorro E, Pérez P (2010) Understanding the high reactivity of the azomethine ylides in [3+ 2] cycloaddition reactions. Lett Org Chem 7:432-439
64. Emamian S (2015) Polar Diels–Alder reaction of isoprene toward 2-bromocyclobutenone followed by a subsequent sodium hydroxide-assisted ring contraction reaction. A regio-and stereoselectivity and molecular mechanism study using DFT. New J Chem 39:9525-9534

Figures

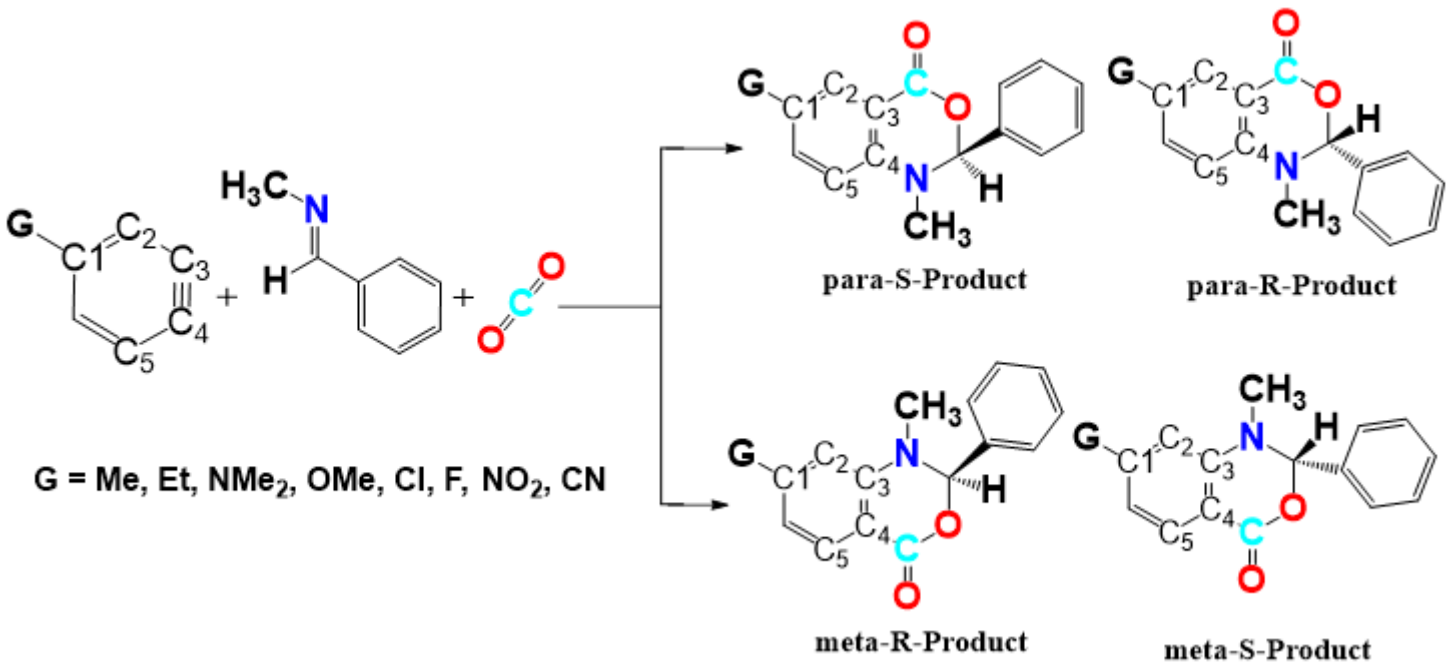

Figure 1

The overall reaction, and the substituted arynes, within atom numbering for the involved atoms in the reaction

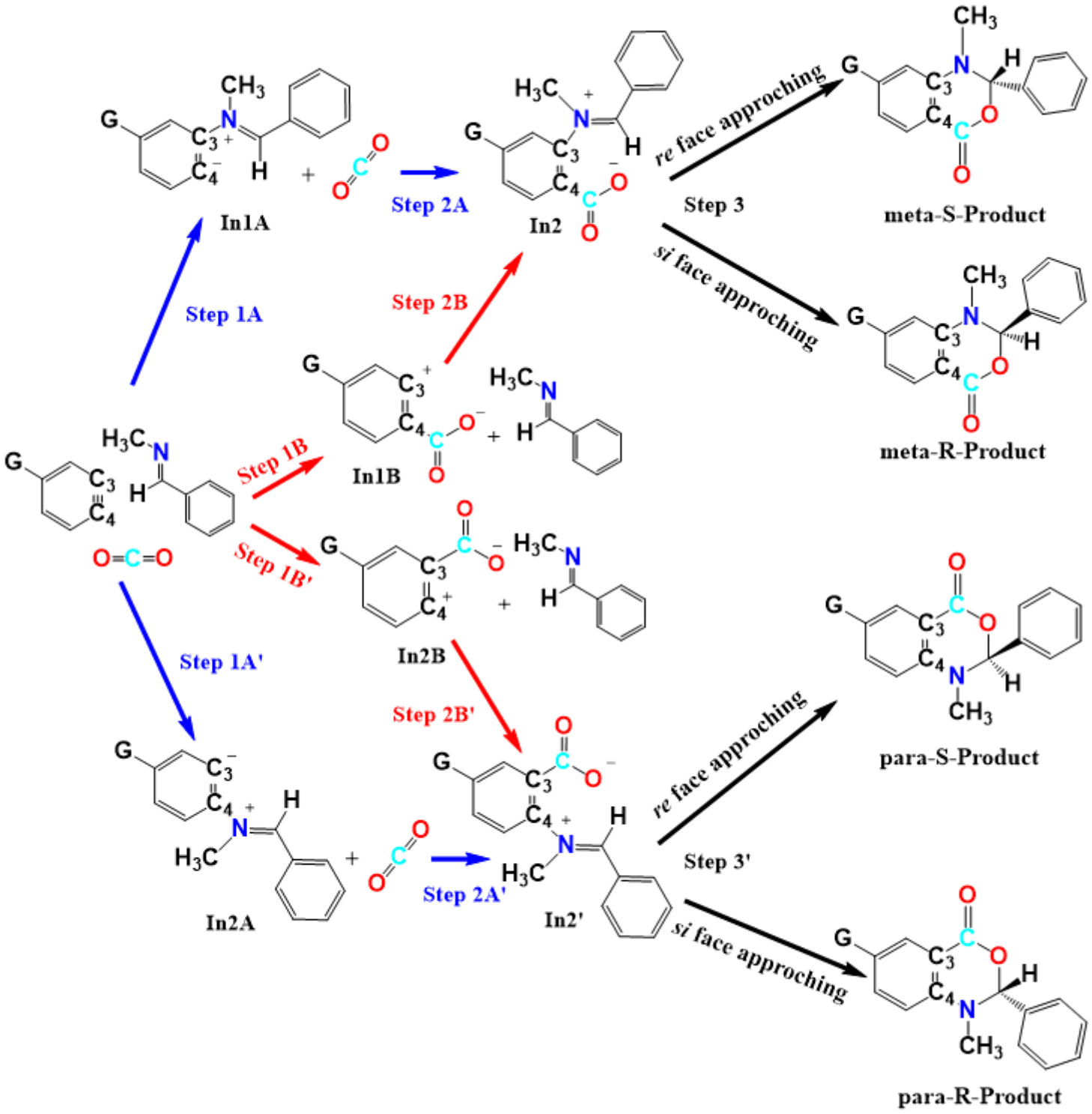

Figure 2

Two possible mechanisms: mechanism A (blue lines) and mechanism B (red lines). Black lines illustrate the common steps of both mechanisms

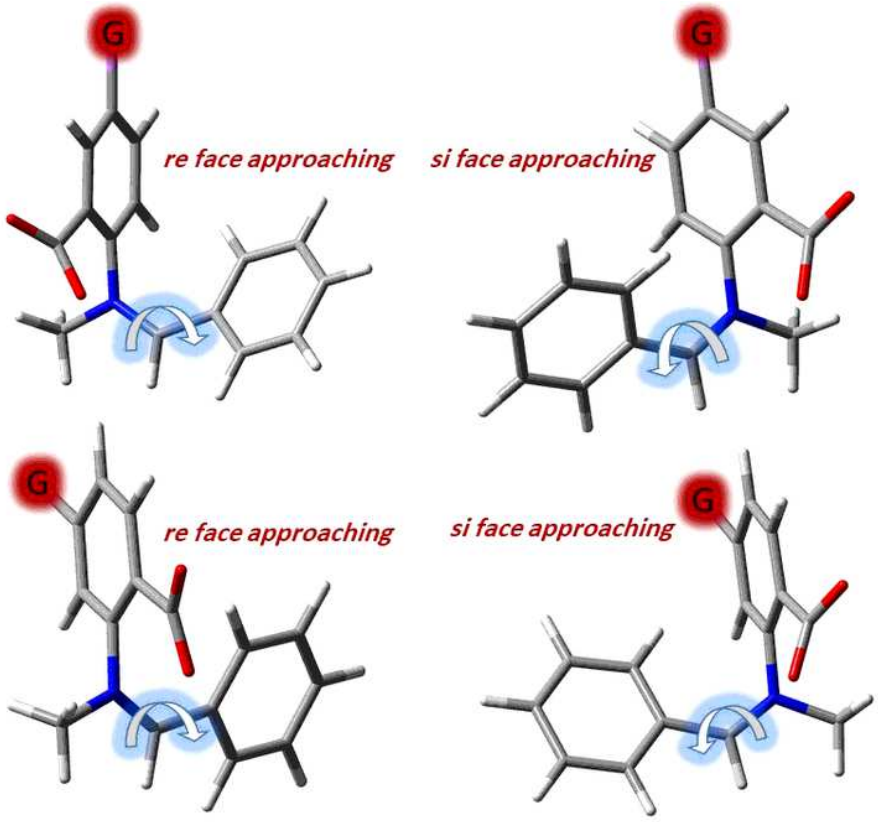

Figure 3

Different nucleophile approaching modes in steps 3 and 3'

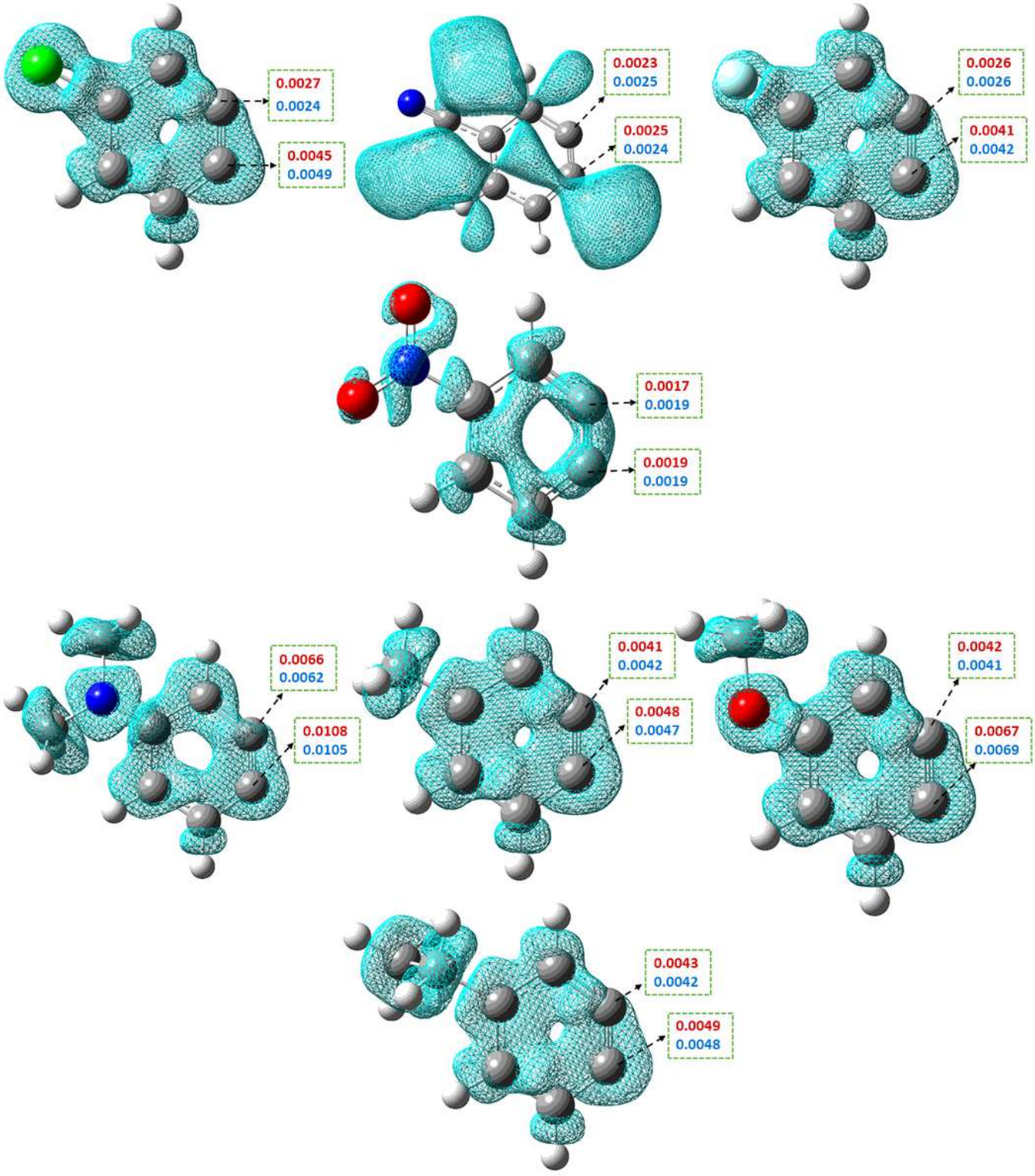

Figure 4

Donor (nucleophilic) Fukui functions isosurfaces and nucleophilicity indexes (Nk) (e) for C4 and C5 atoms at M06-2X/6-31+G(d,p) (Blue color) and M06-2X/6-311++G(2d,p) (Red color) levels.

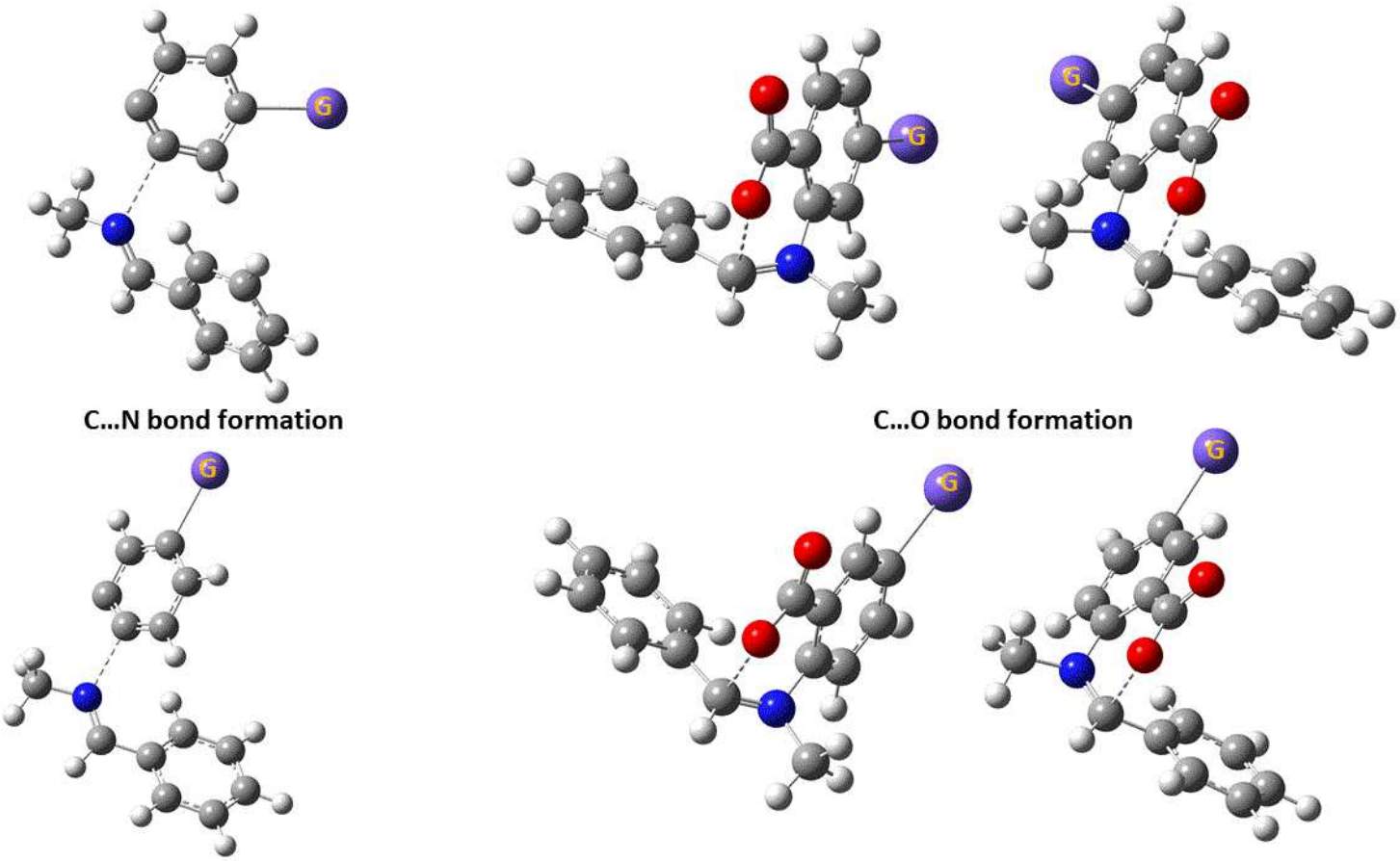

Figure 5

C-N and C-O bond development during the reaction progress through TS1 and TS2 of mechanism A, respectively.

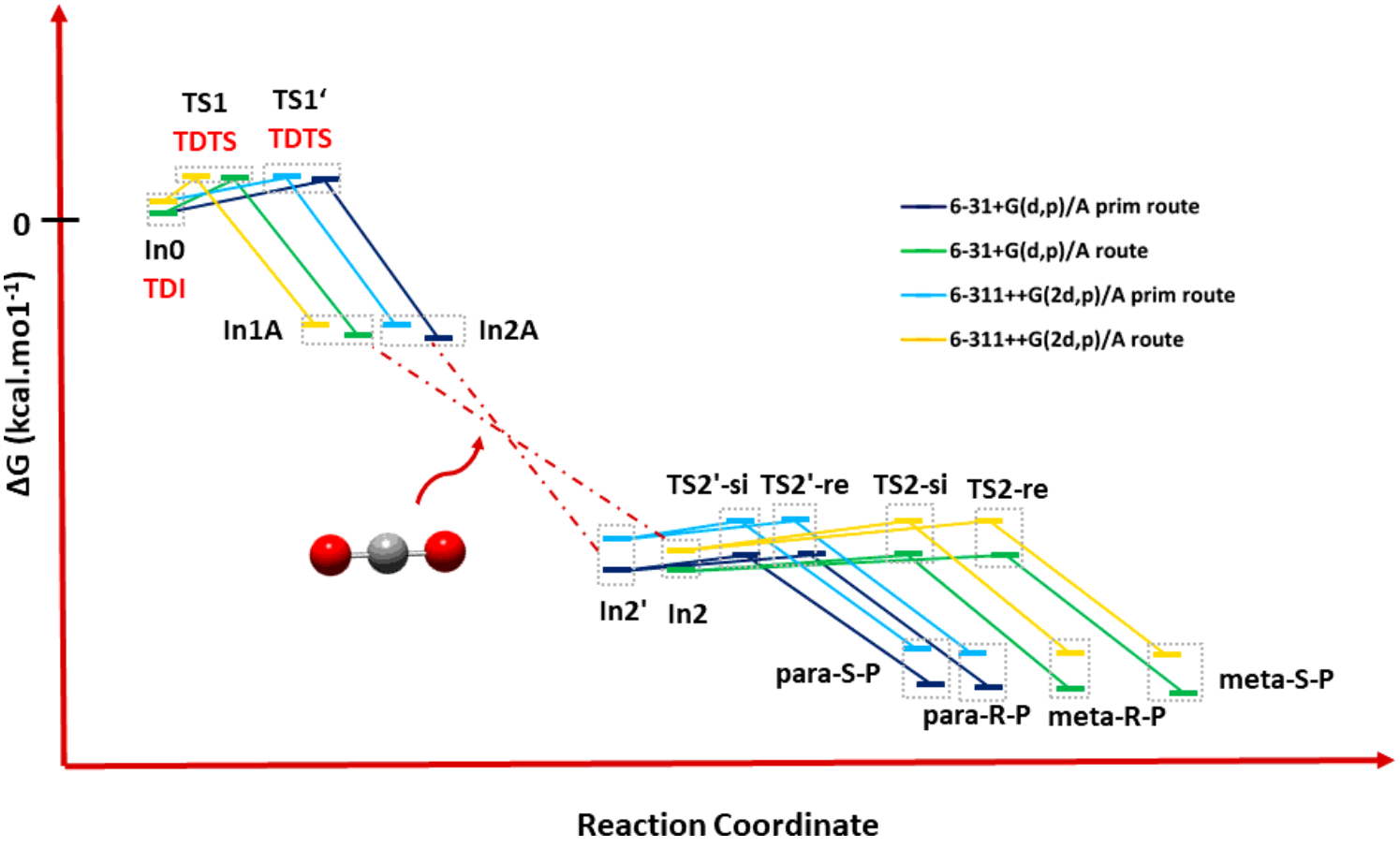

Figure 6

Potential Energy Diagram (PED) for the reaction of Et-substituted aryne

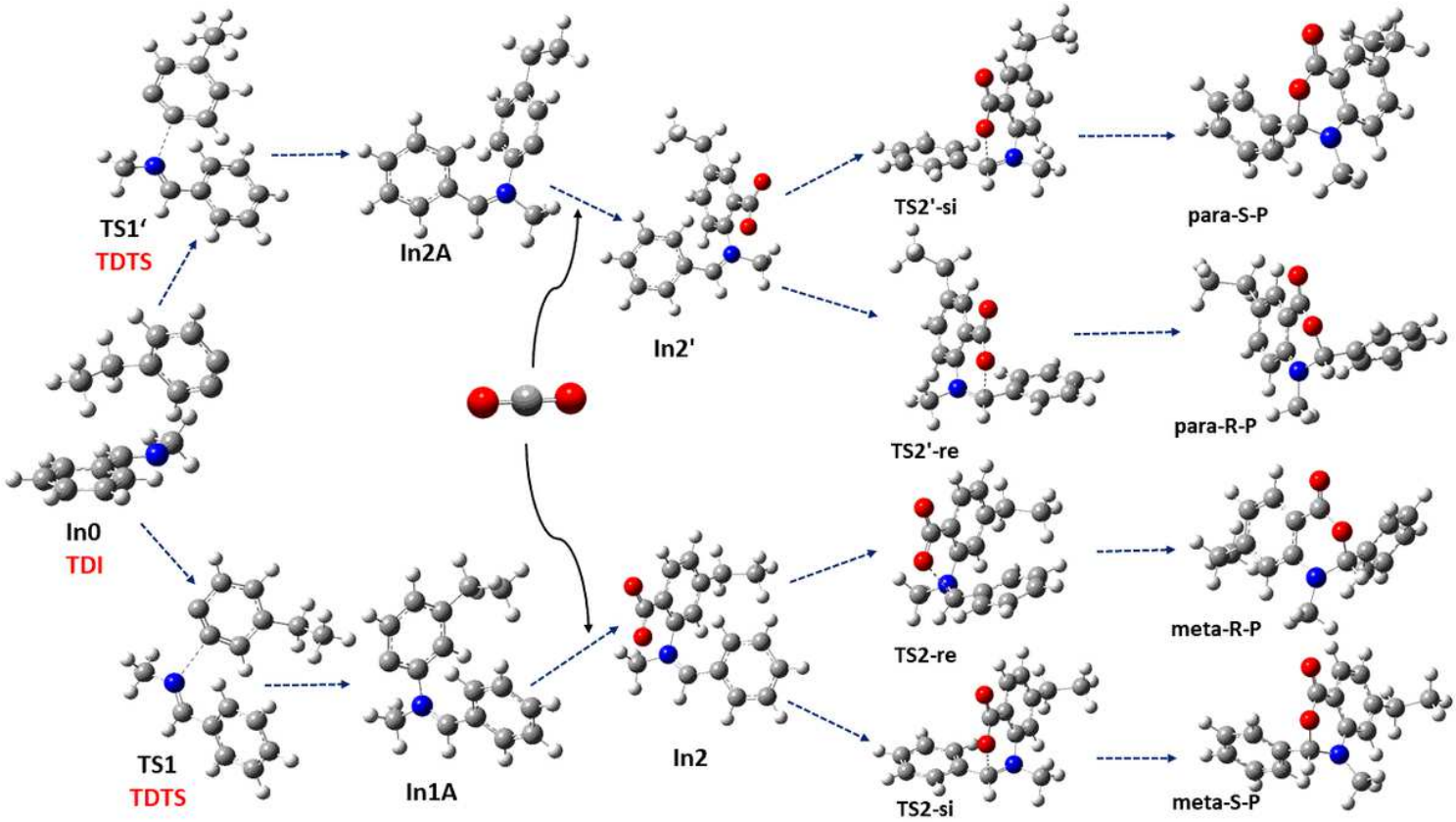

Figure 7

Involved species in the reaction of Et-substituted aryne, as an example

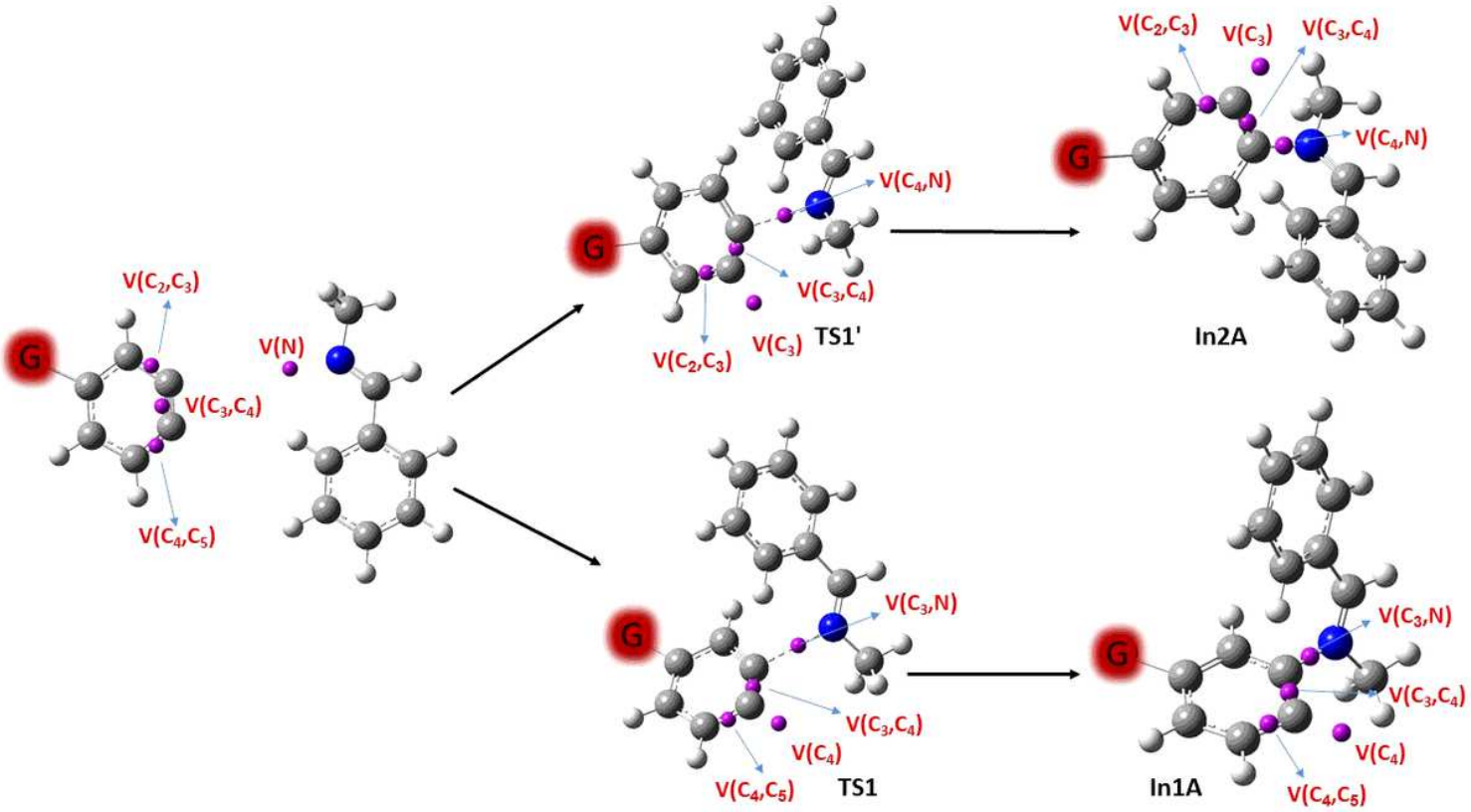

Figure 8

The position of the participating basins in the first steps of both routes in mechanism A

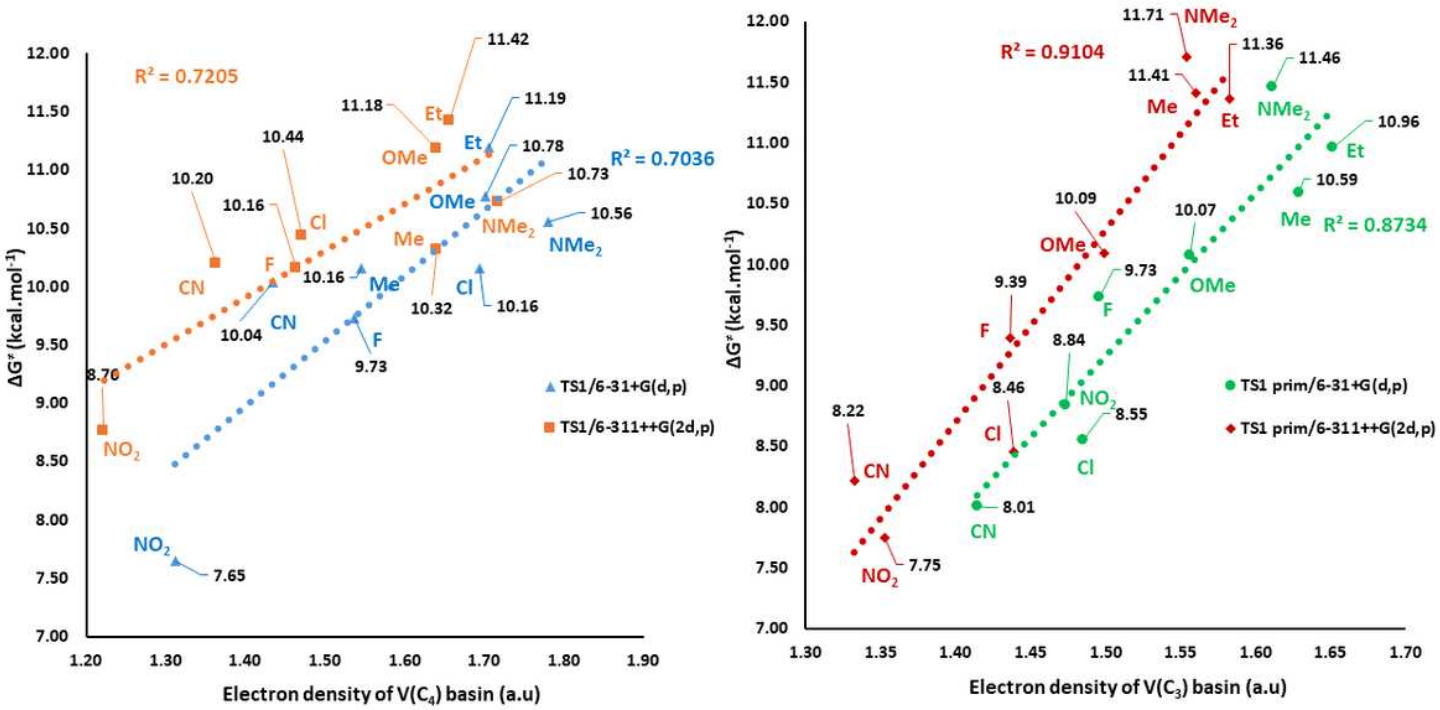

Figure 9

Linear correlation between the electron density of V(C4) and V(C3) basins and ΔG≠ of TDSTs

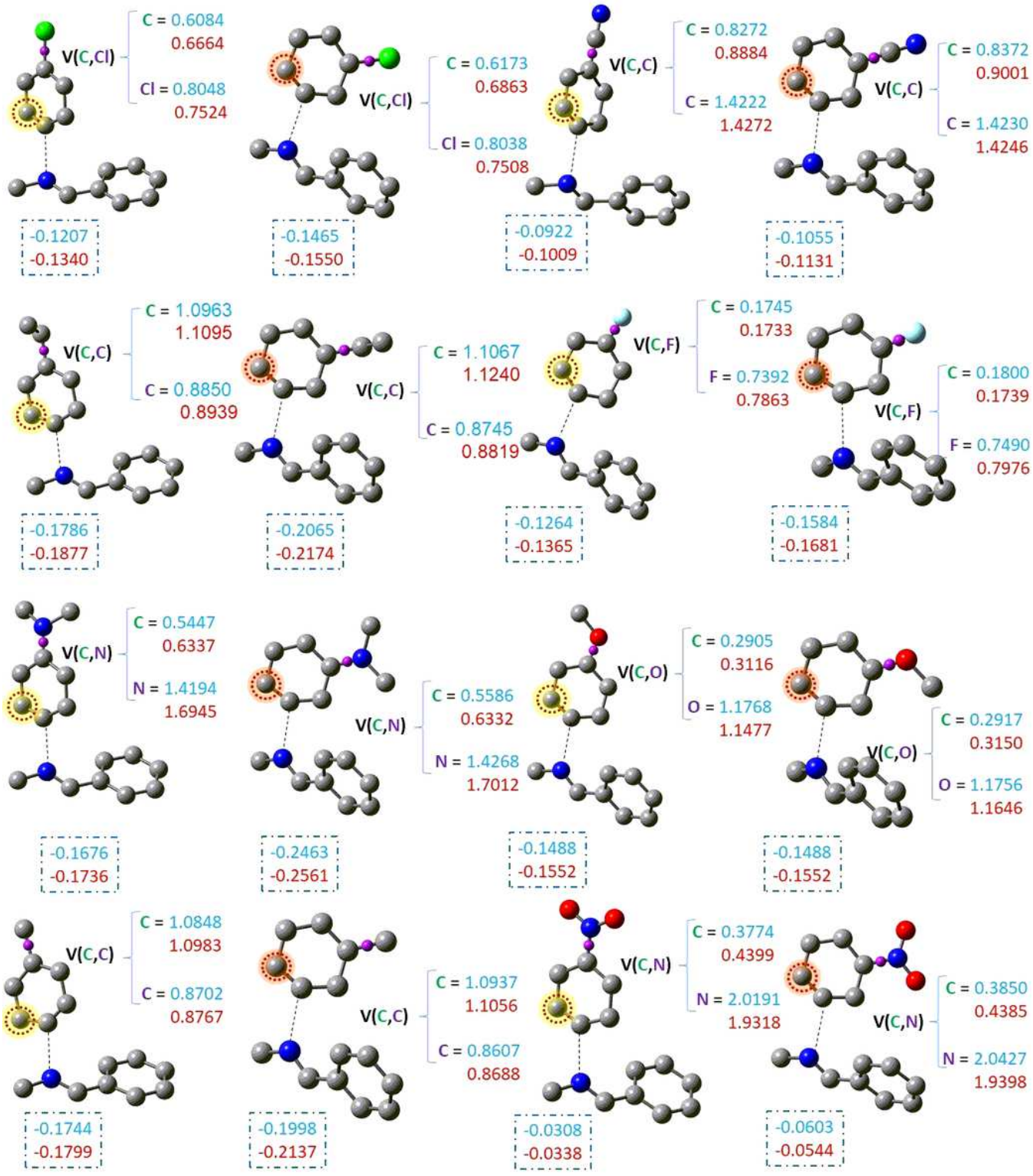

Figure 10

The electron density contributions (in a.u) of C1(in green color) and G (in purple color) atoms in V(C1,G) basins for both TS1 and TS1' and developed natural charges on C3 and C4 atoms at 6-31+G(d,p) (Blue color) and 6-311++G(2d,p) (Red color) levels (Hydrogen atoms have been omitted for more clarity)

Supplementary Files

This is a list of supplementary files associated with this preprint. Click to download.

- Supportinginformation.docx